CENTRO DE INVESTIGACIONES
EN ÓPTICA, A.C.

Stochastic effects in coupled semiconductor and solid-state lasers with coexisting attractors

By:

Alfredo Campos Mejía

Thesis submitted in partial fulfillment of the requirements
for the Ph.D. degree in science (Optics)

Supervised by:

Dr. Alexander Pisarchik

June 2015

Acknowledgments

I express my sincere gratitude to all the people that helped me over the last years at the CIO, and to my colleagues and friends from the Dynamical Systems and Optical Applications Laboratory at the Centro Universitario de los Lagos.

I thank CONACYT, México, for the economical support that made possible for me to participate in this adventure in the quest for new knowledge. I want to give back to society a little bit of all I have received from them through all the academic activities in which I can participate to help to build a sustainable knowledge society that base its welfare on science and technology.

I am very grateful to Dra. Cristina Masoller, Dr. Vicente Aboites, Dr. Yuri Barmenkov, and Dr. Bernardo Mendoza Santoyo, for having accepted to be members of my dissertation jury, for evaluating this work and for their valuable suggestions and constructive criticism.

I especially thank my supervisor, Dr. Alexander Pisarchik, for letting me work in his research group, for his support and professional advice.

Abstract

This thesis is devoted to the experimental study of stochastic effects in multistable semiconductor and solid-state lasers. In the first part, the experimental observation of coherence enhancement of noise-induced intermittency in a semiconductor laser subject to optical injection from another laser at the boundary of the frequency-locking regime is presented. The experimental interspike-interval fluctuations were used to quantitatively characterize the intermittent behavior. In the second part, we study noise-induced intermittency in two mutually coupled semiconductor lasers. Gaussian white noise was applied when both lasers operated in the low-frequency fluctuations regime, near their lasing threshold. The intermittent behaviour of the system output was found, and the type of intermittency analyzed with time series and power spectra. In the third part, we study the dynamics of a dual-cavity Nd:YAG laser with second harmonic generation in one of the cavities and loss modulation in another cavity. We found coexistence of attractors and different dynamical regimes as the frequency of the harmonic modulation of the infrared light was varied.

Thesis overview

The motivation of this work is to contribute to the fundamental understanding of laser dynamics and nonlinear systems, what could lead to the development and improvement of diverse practical applications, not only in the field of secure optical communications, but also in other active research areas of great importance.

The experimental studies presented in this thesis are sorted out in ascending order of the system complexity. We start with an array of two semiconductor lasers with a unidirectional coupling. Next, we present a similar array, but with a bidirectional coupling, and finally, a frequency-doubled Nd:YAG laser with two cavities.

The thesis is organized as follows: chapter 1 gives an introduction to dynamical systems, the basic theories of chaos, lasers, and their connection. We also briefly describe dynamical features of semiconductor lasers, synchronization, multistability and noise-induced effects in lasers. In chapter 2 the experimental investigation of coherence enhancement of noise-induced intermittency in a semiconductor laser subject to optical injection is presented. Chapter 3 describes the study of the noise-induced intermittency observed in mutually coupled semiconductor lasers. Chapter 4 is dedicated to the dynamics of a dual-cavity Nd:YAG laser with second harmonic generation in one of the cavities and loss modulation in the other one. Finally, in chapter 5, the general conclusions and perspectives of this research are given.

Contents

Chapter 1

Introduction

1.1 Dynamical systems

All systems in the world around us are evolving in time, even though sometimes their change is not evident, as the time scales involved could be very different. Their evolution in time may present varied characteristics: a system could move in a particular trajectory to reach at the end a state of stable equilibrium; it could move in cycles over and over, or it could evolve in a very complicated way. In order to describe that behavior quantitatively, mathematical equations are used. Depending on the characteristics of their equations, dynamical systems can be classified into two groups: *iterated maps* (also known as *difference equations* or simply *maps*) and *differential equations*. Iterated maps are used to model systems where time is considered discrete. On the other hand, differential equations describe the evolution of systems in continuous time. Even though realistic systems of considerable importance in science and engineering are modeled by using differential equations, iterated maps are also very useful. For example, they are very helpful to introduce the concept of chaos in a dynamical system and to analyze the solutions of systems described by differential equations.

1.1.1 Nonlinearity

A general framework for ordinary differential equations is provided by the system [1]

$$\begin{aligned} \dot{x}_1 &= f_1(x_1, \ldots, x_n) \\ &\vdots \\ \dot{x}_n &= f_n(x_1, \ldots, x_n) \ , \end{aligned} \tag{1.1}$$

where the overdots represent differentiation with respect to t. The variables $x_1, \ldots, x_n$ could represent concentration of chemicals in a beaker, population of different species

in an ecosystem, the positions and velocities of planets in the solar system, or the dynamical variables describing the output radiation of a semiconductor laser.

The system represented by Equations (1.1) is said to be *linear* if all the x_i on the right-hand side appear to the first power, that is, if every term on the right-hand side is linear in x_i. Otherwise, the system is called *nonlinear* Examples of nonlinear terms are products, powers and functions of the x_i, such as: $x_1 x_3$, x_1^2, or $\sin(x_1)$. Nonlinearity is crucial in the operation of a laser. In fact, most dynamical systems in nature are nonlinear. When parts of a system cooperate, interfere or compete, nonlinear interactions are taking place.

Linear systems can be broken down into parts, then each part can be solved separately, and the partial solutions can be recombined to obtain the general solution. On the other hand, in nonlinear systems the superposition principle fails, and their equations are generally difficult to solve analytically. Fortunately, nonlinear systems can be usually approximated by linear equations, a process that is called *linearization*.

1.1.2 Phase space

The abstract space with coordinates $(x_1, \ldots, x_n)$ is called the *phase space* for the dynamical system, and its temporal dynamics can be represented in this space. The phase space is a very useful tool to visualize and analyze the dynamical behavior of a system. If we consider as an example a system with $n = 2$, where x_1 and x_2 represent the position and the velocity of an object, respectively, then the solution $(x_1(t), x_2(t))$ corresponds to a point moving along a curve in this particular space, as shown in Figure 1.1.

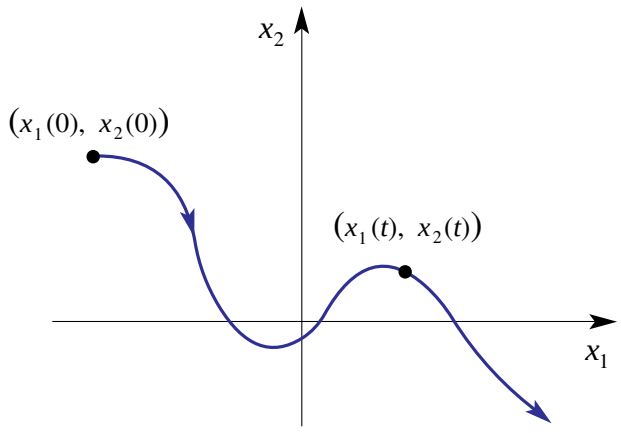

Figure 1.1: Trajectory followed by a point moving along a curve in the space with coordinates $(x_1(t), x_2(t))$ and initial condition $(x_1(0), x_2(0))$

That curve is called a *trajectory* or an *orbit*. Since each point in phase space could serve as an initial condition, the phase space is completely filled with trajectories. However, in practice, the set of initial conditions for a real system is limited. The orbit may converge into a shape or *attractor* in phase space. For example, for a constant value of the variables, the attractor becomes a point in phase space. For some oscillating systems, the trajectory could be closed, with a circular orbit as a particular case. A closed trajectory in phase space is known as a *limit cycle*.

The system represented by Equations (1.1), is referred to as an *n-dimensional system* or an *nth order system*. Some examples of phenomena that can be modeled by linear systems are: the exponential grow ($n = 1$), the radioactive decay ($n = 1$), an oscillating mass on a spring ($n = 2$), and an RLC circuit ($n = 2$). A classical and well known example of a nonlinear system is a pendulum ($n = 2$).

1.1.3 Fixed points

In order to analyze the dynamics of a system, it is very useful to find its *fixed points*, that is, the values of a dynamical variable for which its temporal evolution remains stationary. Fixed points can be easily found geometrically for a one-dimensional system if differential equations are interpreted as vector fields. To understand this procedure, let us consider the following nonlinear differential equation

$$\dot{x} = x^2 - 1 \; . \tag{1.2}$$

If we think of t as time, x as the position of an imaginary particle moving along the real line, and $\dot{x}$ as the velocity of that particle, then Equation (1.2) represents a vector field on the line, as it assigns a velocity vector $\dot{x}$ for each position x. To sketch the vector field, we plot $\dot{x}$ versus x, and then we draw arrows on the x-axis to indicate the velocity vector at each x. The arrows point to the right when $\dot{x} > 0$, and to the left when $\dot{x} < 0$. If we imagine that the arrows represent the direction of some sort of "fluid" that is flowing along the x-axis, the flow is to the right when $\dot{x} > 0$ and to the left when $\dot{x} < 0$. At points where $\dot{x} = 0$, there is no flow. These special points are called *fixed points*. As shown in Figure 1.2, solid black dots represent a *stable* fixed point (also referred to as attractors or sinks) and open circles represent *unstable* fixed points (also referred to as repellers or sources).

Fixed points represent equilibrium solutions of differential equations. An equilibrium is defined to be stable if small disturbances away from it damp out in time. Some examples of stable equilibrium are the bottom position of a damped pendulum and the bottom of a bowl containing a rolling marble. Thus, stable equilibrium

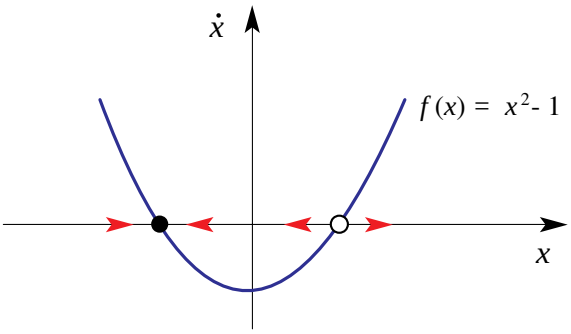

Figure 1.2: Trajectory in phase space for the dynamical variables of a system showing two fixed points. The stable fixed point is represented by the black dot and the unstable fixed point by the open circle.

is represented by a stable fixed point. Conversely, unstable equilibrium, in which disturbances grow in time, is represented by an unstable fixed point [1].

1.2 Basic chaos theory

In science, the word *chaos* is used to describe fluctuations (time-varying or space-varying irregular phenomena) that are governed by a deterministic rule, and can be described by using mathematical equations. Chaos is a dynamical state present in a wide variety of systems in many fields, including fluids, plasmas, solid-state devices, circuits, lasers, mechanical devices, etc. [2]. In order to describe the basic properties of chaos, it will be helpful to describe the logistic map and the Lorenz model.

1.2.1 Iterated maps

A *discrete sequence* is a set of numbers $x_0, x_1, \ldots, x_n, \ldots, x_N$, where $n = 0, 1, \ldots, N$. An iterated map can be defined by a function f that relates x_{n+1} with x_n for all n, that is

$$x_{n+1} = f(x_n) \, . \tag{1.3}$$

First, x_1 can be obtained from x_0 by using Equation (1.3), when x_0 is given as an *initial condition*. Then, x_2 is obtained from x_1, x_3 is obtained from x_2 and so on. In this sense, the map is completely deterministic by using the rule given by Equation (1.3) and the chosen initial condition x_0.

1.2.1.1 The logistic map

One of the simplest models to exhibit chaos is the logistic map [3]. It is the discrete version of the *logistic equation*, a continuous-time differential equation that has been used as a demographic model and was published by Pierre François Verhulst in 1838. The logistic map is written as

$$x_{n+1} = a x_n (1 - x_n) \ , \tag{1.4}$$

where a is a control parameter for the map, $n = 0, 1, 2, \ldots, N$, and $0 \leq x_n \leq 1$. A typical value of the parameter to observe chaos is $a = 4$. As can be seen in Figure 1.3, the sequence of the discrete variable x_n shows an irregular behavior, even though Equation (1.4) is very simple and completely deterministic. It might seem that if the rule and the initial condition are known, this irregular sequence could be completely predicted because it was derived from a deterministic rule. This is true in theory, however, an initial condition with "infinite" precision would be necessary to be able to make a long term prediction, which is impossible for real chaotic dynamical systems. This leads to another very important characteristic of deterministic chaos, known as *sensitive dependence on initial conditions* [4], which means that if two chaotic sequences start from very close but slightly different initial conditions, the two sequences would be very similar at the beginning, but then they would start to diverge exponentially and would never show the same behavior again. This is the reason why it is impossible to predict the output of a chaotic system in the long-term.

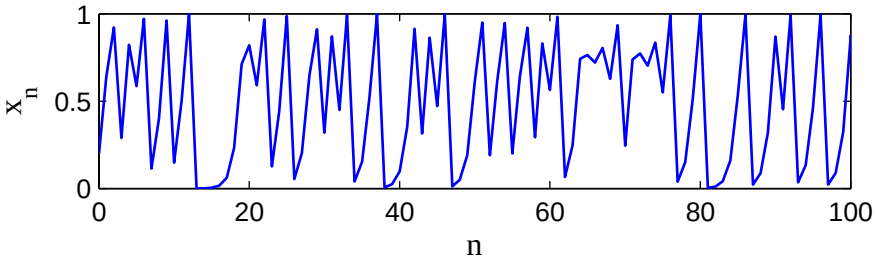

Figure 1.3: Sequence of the discrete variable x_n in the logistic map for $a = 4$ and $x_0 = 0.2$.

1.2.2 Bifurcations

Another characteristic of chaos is a transition among different dynamical states. *Bifurcations* are the qualitative changes in the dynamics experienced by a dynamical

system when a small smooth change is made to the control parameter, and the parameter values at which they occur are called *bifurcation points*. Bifurcations provide models of transitions and instabilities as a control parameter of a system is varied. For example, bifurcations can help to model phenomena such as the start of coherent emission of radiation in a laser, the outbreak of an insect population, etc. There are many kind of bifurcations [1,2]. In this section, some of them will be briefly described.

1.2.2.1 Saddle-node bifurcation

The saddle-node bifurcation is the basic mechanism by which fixed points are created and destroyed. As a control parameter is varied, two fixed points move toward each other, collide and annihilate. This bifurcation can be illustrated by means of the following first-order system

$$\dot{x} = r + x^2 \ , \tag{1.5}$$

where r is a parameter that can take any real value. When r is negative, there are two fixed points, one stable $(-\sqrt{r})$ and one unstable $(+\sqrt{r})$, as shown in Figure 1.4(a). As r approaches 0 from negative values, the parabola moves up and the two fixed points approach to each other. When $r = 0$, the fixed points combine into a half-stable fixed point at $x = 0$ (Figure 1.4(b)). This type of fixed point vanishes as soon as $r > 0$, leaving no fixed points at all (Figure 1.4(c)).

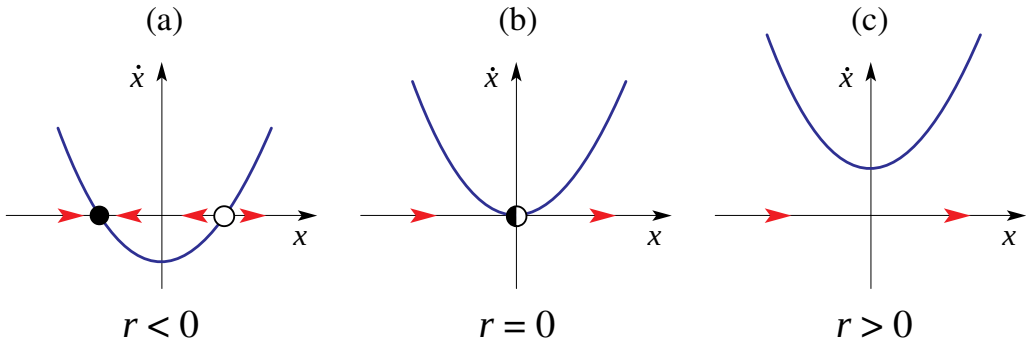

Figure 1.4: Geometrical representation of the saddle-node bifurcation. (a) When r is negative, there are two fixed points, one stable (the black dot) and one unstable (the open circle). (b) When $r = 0$, the fixed points combine into a half-stable fixed point. (c) When $r > 0$, the half-stable fixed point vanishes.

There are other ways to depict a saddle-node bifurcation. One very common way is shown in Figure 1.5, where the parameter r plays the role of an independent

variable, and for that reason is plotted horizontally. The x-axis has now to be plotted vertically, what could look strange at first. To distinguish between stable and unstable fixed points, a solid line for stable points is used, and a dashed line for unstable ones. Now, if we imagine a vertical line for a particular value of r, we can find the fixed points as the intersections between this line and the two branches of the parabola. This representation is called the *bifurcation diagram* for the saddle-node bifurcation.

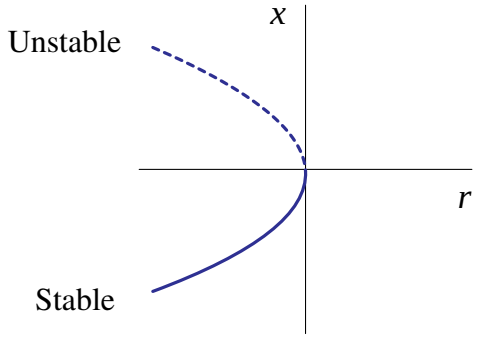

Figure 1.5: Saddle-node bifurcation representation. The solid line represents stable points, and the dashed line unstable ones.

1.2.2.2 Period-doubling bifurcation

This type of bifurcation occurs when a system has a periodic solution. As a control parameter is increased, it reaches a point when the initial period is doubled. As a result, an initially stable periodic orbit is transformed into a stable periodic orbit with the period doubled, and an unstable periodic orbit. The *bifurcation diagram* for the period-doubling bifurcation is shown in Figure 1.6. The axes have been omitted to simplify the diagram, but the horizontal axis represents the values of the system control parameter.

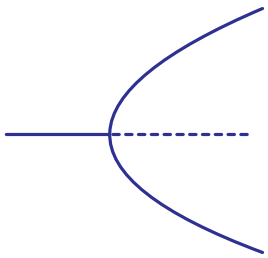

Figure 1.6: Period-doubling bifurcation. An initially stable periodic orbit is transformed into a stable periodic orbit with the period doubled, and an unstable periodic orbit as the control parameter is increased.

1.2.2.3 Inverse period-doubling bifurcation

It this bifurcation, as a control parameter is changed, an initially unstable periodic orbit is transformed into an unstable periodic orbit with the period doubled and a stable periodic orbit (Figure 1.7).

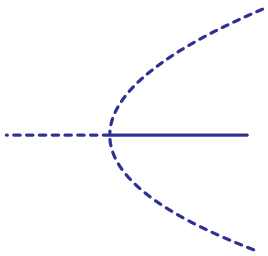

Figure 1.7: Inverse period-doubling bifurcation. An initially unstable periodic orbit is transformed into a unstable periodic orbit with the period doubled and an stable periodic orbit as the control parameter is increased.

1.2.2.4 Hopf bifurcation

In a Hopf bifurcation, a fixed point of a dynamical system loses stability as the control parameter varies, and the dynamics of the system changes into a period-1 orbit. As the control parameter value is increased, the amplitude of the periodic solution increases too.

1.2.2.5 Bifurcation diagram of the logistic map

In the logistic map, when the value of parameter a is changed, distinct states can be obtained. Different number of values of x_n are obtained at different values of the control parameter a: one constant value (Figure 1.8(a), $a = 2.5$), two different values (Figure 1.8(b), $a = 3.25$), four different values (Figure 1.8(c), $a = 3.5$), and irregular aperiodic values (Figure 1.8(d), $a = 4$). For this reason, these dynamical states are called period-1, period-2, period-4, and chaos, respectively.

Figure 1.9 shows the bifurcation diagram of the logistic map when the parameter a is changed. To create the bifurcation diagram, some values of x_n are plotted along the vertical axis at a fixed value of a. Then, a is increased and some values of the new x_n are plotted again at a new fixed a. This procedure of changing a and plotting x_n is repeated. The bifurcation diagram in Figure 1.9 shows different dynamical states of the sequences. For example, x_n is a single value (corresponding to a period-1 sequence) at the region of $1 \leq a \leq 3$. Then, two values of x_n appear (period-2

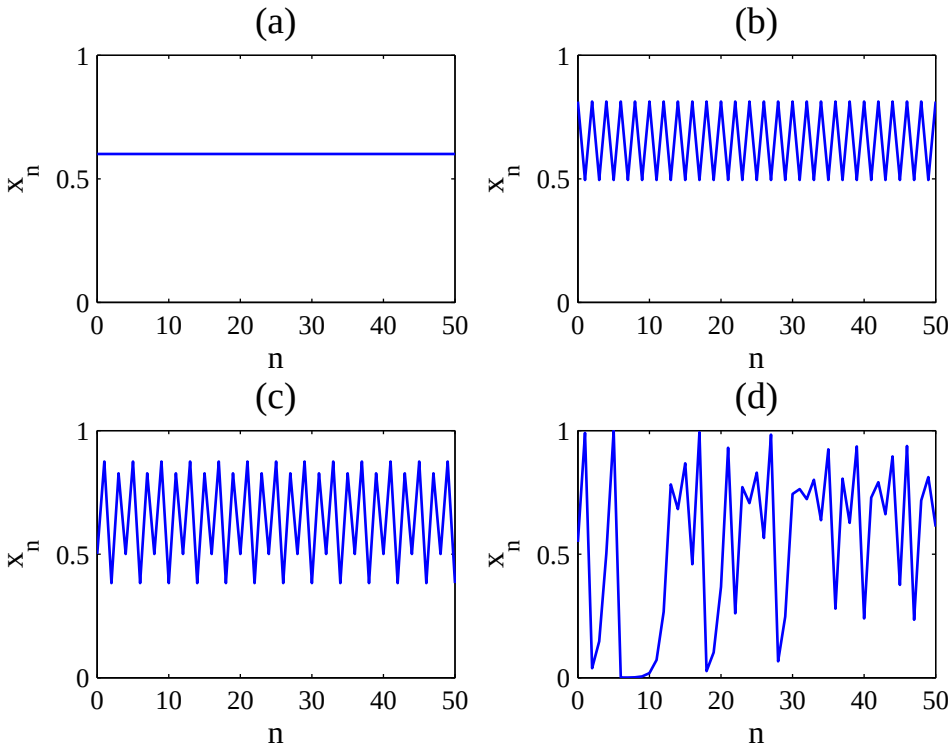

Figure 1.8: Sequences of x_n at different values of the control parameter a in the logistic map. (a) Period-1 ($a = 2.5$), (b) period-2 ($a = 3.25$), (c) period-4 ($a = 3.5$), and (d) chaos ($a = 4$).

sequence) in the region of $3 \leq a < 3.4494\ldots$. After that region, four values of x_n are observed (period-4), followed by eight values (period-8), and so on. Finally, for $a > 3.5699\ldots$ irregular values of x_n (chaos) are obtained.

1.2.3 Chaos in a continuous-time system

More realistic models can be developed by using a set of coupled ordinary differential equations in continuous-time dynamical systems. A classical example of a model of this kind that exhibits chaos is the Lorenz model [4], which consists of three coupled ordinary differential equations that describe the fluid convection in a cell heated from below and maintained at a lower temperature on the top. Figure 1.10(a) shows the temporal waveform (also called *time series*) of one of the variables of the Lorenz system that displays chaotic irregular fluctuations. In continuous-time dynamical systems, it has been shown that at least three independent variables (i.e. three degrees of freedom) are necessary to observe deterministic chaos [1]. This is the case

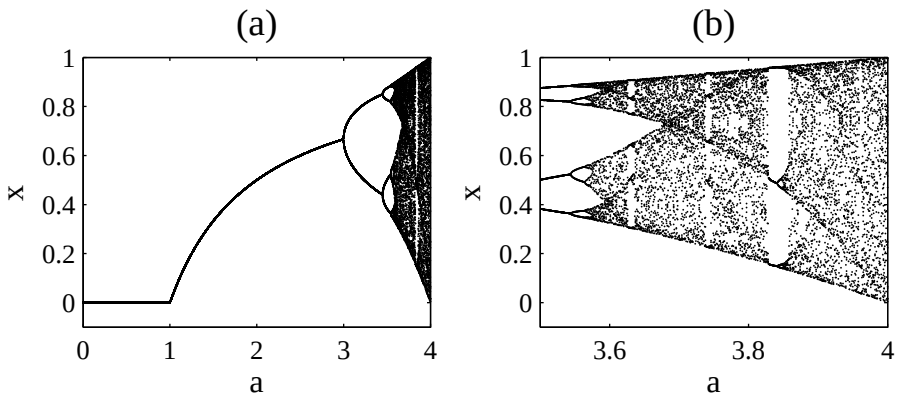

Figure 1.9: (a) Bifurcation diagram of the logistic map when a is changed from 0 to 4. (b) Amplification of (a) from $a = 3.5$ to $a = 4$.

for the Lorentz model, which has three degrees of freedom and nonlinear terms that make possible the generation of a chaotic dynamical behavior.

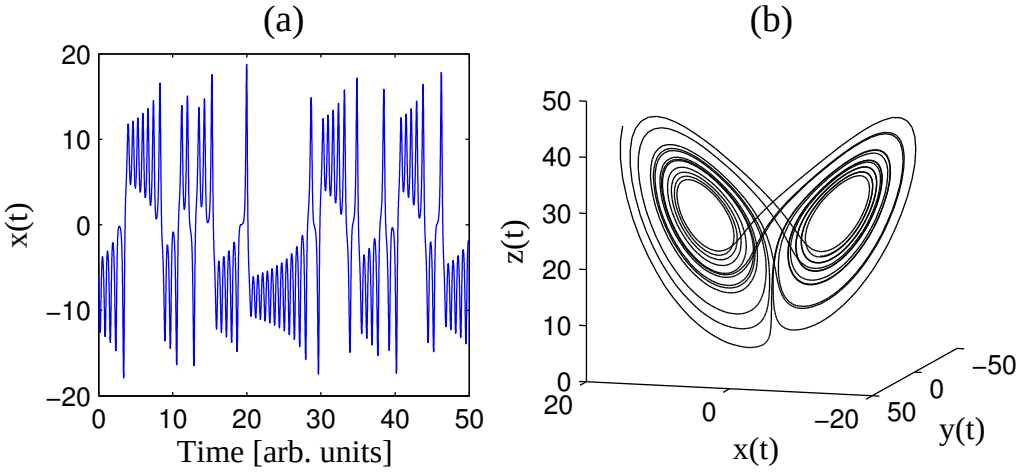

Figure 1.10: (a) Time series for the variable $x(t)$ in the Lorenz model showing a chaotic behavior. (b) The Lorenz attractor obtained when the three variables ($x(t)$, $y(t)$, and $z(t)$) of the Lorenz model are plotted.

The temporal dynamics of the Lorenz system is represented in phase space in Figure 1.10(b), where their three variables are plotted. The trajectory converges into a characteristic shape or attractor at $t \to \infty$. For chaotic oscillations, the attractor resembles a strange shape, as seen in Figure 1.10(b). For that reason, these kind of attractors are called *chaotic attractors* or *strange attractors*.

1.2.4 Routes to chaos

A *route to chaos* is another important feature of deterministic chaos that consists in a transition from a steady state to chaos through various states when the value of a system parameter is changed. There are three types of routes to chaos observed in many dynamical systems: the *period-doubling* route, the *quasiperiodic* route, and the *intermittency* route. These routes to chaos have been observed in many laser systems, and have been used to identify the existence of deterministic chaos in laser experiments.

1.2.4.1 Period-doubling route to chaos

This route to chaos starts from a steady state, a period-1 oscillation, a period-2 oscillation, a period-4 oscillation, ..., a period-$2n$ oscillation (n is a positive integer), ..., to reach eventually a chaotic oscillation. The period-doubling route to chaos has been observed in many discrete systems, like the logistic map, and also in continuous-time dynamical systems. It has been observed in laser experiments and simulations.

1.2.4.2 Quasiperiodic route to chaos

The quasiperiodic route to chaos starts from a steady state, a period-1 oscillation, a quasiperiodic oscillation, and a chaotic oscillation. Quasiperiodic oscillations can be identified by observing the appearance of two frequencies with incommensurable ratio in the frequency spectrum. This route to chaos is observed in a laser system with external modulation, since two characteristic frequencies, which are internal (the relaxation oscillation) and external (the modulation), interact with each other nonlinearly and induce chaotic instabilities.

1.2.4.3 Intermittency route to chaos

The intermittency route to chaos may be observed in a dynamical system when a control parameter passes through a critical point. The intermittent behaviour is characterized by irregular bursts interrupting a nearly regular state, as can be seen in Figure 1.11. The mean duration of the regular states decreases as the control parameter is increased beyond the critical value, and eventually the regular states disappear. Intermittency will be treated in more detail in chapter 3, which deals with its experimental observation and characterization.

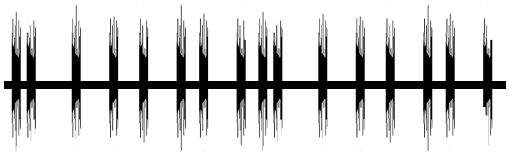

Figure 1.11: Intermittency in the dynamical behavior of a system is characterized by irregular bursts interrupting a nearly regular oscillation or steady state. This figure shows a qualitative example of a system exhibiting intermittency in one of its dynamical variables. The regular steady state is interrupted nonperiodically by amplitude fluctuations (the bursts). The waveform can be thought as a sequence of laminar phases (the windows of steady state) and turbulent phases (the windows of irregular behavior).

1.3 Basic laser theory

The term of *laser* is the acronym for Light Amplification by Stimulated Emission of Radiation. Besides natural lasers (astrophysical or space lasers [5]), on Earth, a laser is an artificial light source that generates *coherent* light, which indicates the identical phase state of the photons. This coherent emission enhances the brightness of light, the ability to produce light interference and the narrow optical spectrum of the laser. In 1917, Albert Einstein established the theoretical foundations for the laser [6], and in 1953 Charles H. Townes and coworkers developed the first device that operated under these principles, named *maser* because it was a coherent source of microwaves [7]. In 1960, only seven years later, Theodore H. Maiman made reality the first laser operating at a visible wavelength based on a ruby crystal (Al_2O_3:Cr). This laser produced a red beam of light at 694 nm [8].

The laser can be considered as one of the most important inventions in the twentieth century, that has made possible new technologies such as optical communications, optical storage of information, material processing, precise measuring, medical applications, remote sensing, among many others [9].

1.3.1 Laser elements

There are three key components in a laser: a laser medium, a laser cavity and a pump mechanism, as shown in Figure 1.12. The laser medium, which can be a semiconductor, a fiber, a gas or a solid-state material, provides light amplification and is inserted into the laser cavity, which consists of a pair of reflecting mirrors that confine the generated light. The pump energy is transferred to the laser medium by using a flash lamp, a laser light, or an an electric current. The pump energy excites

the atoms in the laser medium, which in turn can amplify the light that is directed to them [10].

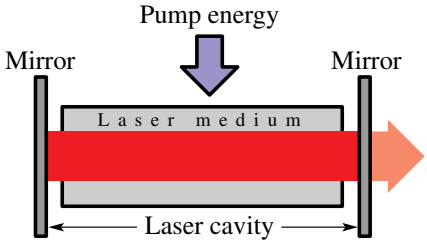

Figure 1.12: Basic elements of a laser system. The laser medium is inserted into the laser cavity that consists of a pair of mirrors, and a pump energy is applied to the laser medium.

The amplifying medium is usually enclosed by the cavity that holds the amplified light, redirecting it through the medium for repeated amplification. The energy of the amplifier that is being converted to light needs to be added continuously. The generated light in the form of a beam in the cavity is extracted from one of the mirrors that is partially transparent to the laser light.

1.3.2 Two-atomic-level description of the laser oscillation

Let us consider the process of generation of coherent light in the laser medium by using a simplified two-level model, as shown in Figure 1.13. By some pumping mechanism some of these atoms are promoted from the ground level to the excited level. It is said that a *population inversion* is produced when the number of atoms in the excited level is larger than the one in the ground level. Even though this scheme is very useful for illustrative purposes, more than two atomic levels are required to attain the population inversion in real laser systems [11, 12]. The excited atoms begin radiating *spontaneous emission*, for which a photon is produced spontaneously from an excited atom when it decays to the ground level. A photon produced in this way can induce an excited atom to emit another photon of the same frequency, phase, polarization state, and direction as the first, which is referred to as *stimulated emission*. The mirrors of the laser cavity keep most of the photons from escaping, so that they can be redirected back to the active laser medium to stimulate the emission of more photons. By making the mirrors partially transmitting, some of the photons are allowed to escape. These photons constitute the output laser beam, whose intensity is determined by the rate of production of excited atoms (the population-inversion lifetime) and the loss of the photons in the laser cavity and the active medium (the photon lifetime). When the pumping power is enough to produce the population inversion while photons are generated by stimulated emission, continuous laser output is obtained [10].

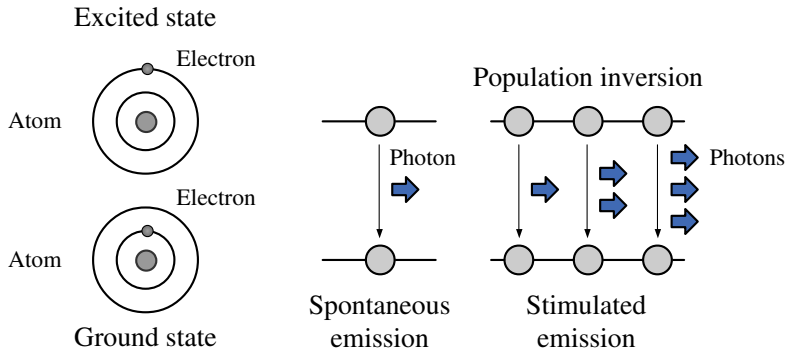

Figure 1.13: Principle of laser oscillation in a two-atomic-level. By a pumping mechanism, some of the atoms are promoted from a ground state to an excited state. The excited atoms begin to radiate spontaneous emission, that in turn can induce an excited atom to emit another photon of the same frequency, polarization, phase, and direction as the first.

1.3.3 Semiconductor lasers

Semiconductor lasers (also referred to as *diode lasers*) are optical devices that convert an electric current (the pump energy) into coherent light. Since their development in 1962 [13], semiconductor lasers have found multiple applications in science and technology due to their unique properties [14]:

- Low power consumption.
- Small size (the typical length of a semiconductor laser is 0.25 mm).
- Reliability.
- Ease of fabrication.
- High frequency modulation (more than 10 GHz).
- Long service life.
- Low cost.
- Wide range of emission wavelengths.

One of the most outstanding uses of semiconductor lasers is as light sources for optical fiber communication systems, designed to transmit a huge amount of information at long distances. They are also widely used for optical data storage in CDs, DVDs and Blu-ray systems. Other domains in which semiconductor lasers have found important applications are optical metrology, spectroscopy, medicine, material processing, air pollution monitoring, etc. Nowadays, they are ubiquitous in portable pointers.

1.3.3.1 Radiative recombination of electron-hole pairs

The basic structure of semiconductor lasers is the p-n junction, formed by bringing a p-type (with many holes) and a n-type (with many electrons) semiconductor into contact with each other. When a p-n junction is forward-biased by applying an external voltage, the built-in electric field is reduced, what makes possible the diffusion of electrons and holes across the junction. In a narrow depletion region, both electrons and holes are present simultaneously and can recombine either radiatively or nonradiatively. During radiative recombination photons are emitted. However, these photons can also be absorbed through a reverse process that generates electron-hole pairs. When the external voltage surpasses a critical value, a condition known as population inversion is achieved, in which the rate of photon emission exceeds that of absorption. The p-n junction is then able to amplify the electromagnetic radiation. The amount of electron-hole pairs is also referred to as the *carrier density*, which is proportional to the injection current of the semiconductor laser. To obtain high gain of the amplification in semiconductor lasers, a p-n heterojunction structure is used. Electrons and holes can move freely to the active region under forward bias. However, once there, they cannot cross over to the other side because of the potential barrier resulting from the bandgap difference. This enhances the electron and hole population inside the active region, where they can recombine to produce optical gain. In semiconductor lasers, the optical feedback is usually implemented by cleaving the semiconductor along its crystal planes. The Fresnel reflections between the semiconductor ($n \sim 3.5$) and air ($n \sim 1$) cause facet reflectivities of about 30%, which is sufficient for lasing action to occur in diode lasers of usual length (0.25 mm), so the laser does not need additional mirrors [14].

1.3.4 Nd:YAG lasers

Besides ruby lasers, there are many solid-state lasers, though not many in the visible region. The most common are the rare-earth ions in crystals or glasses, like Nd^{3+} lasers using Nd:YAG (Nd^{3+} ions in yttrium aluminum garnet) materials, in which the neodymium ion provides the lasing activity in the crystal. Nd:YAG absorbs mostly in the bands between 730–760 nm and 790–820 nm, and Nd:YAG lasers are pumped using a flashtube or laser diodes that emit at these particular wavelengths. Nd:YAG lasers typically emit at 1064 nm, and can operate in both pulsed and continuous mode.

The operation of the Nd:YAG laser was first demonstrated in 1964 [15], and since that moment it has found multiple applications in medicine, industry, and science [11].

1.3.5 Rate equations for laser dynamics

The temporal dynamics of lasers can be described by using a set of coupled ordinary differential equations, where the main three physical variables are the *electric-field*, the *population inversion*, and the *atomic polarization* of the laser medium. The rates of these three physical variables are governed by physical laws in the laser cavity and described by a set of mathematical formulas, known as *rate equations*. One of the simplest formula for the dynamics of a model of two-level atoms is described as follows [16]

$$\frac{dI(t)}{dt} = gI(t)N(t) - \frac{I(t)}{\tau_p} , \tag{1.6}$$

$$\frac{dN(t)}{dt} = R - gI(t)N(t) - \frac{N(t)}{\tau_s} , \tag{1.7}$$

where $I(t)$ is the laser intensity (described by a real number) and $I = |E|^2$, $N(t)$ is the population inversion [m^{-3}], g is the laser gain [$m^3\ s^{-1}$], R is the pump energy for lasing [$m^{-3}\ s^{-1}$], τ_p is the photon lifetime [s], and τ_s is the population lifetime [s]. Equation (1.6) describes the temporal dynamics of the laser intensity $I(t)$, and Equation (1.7) models the dynamics of the population inversion $N(t)$. In Equations (1.6) and (1.7), the product of $I(t)$ and $N(t)$ exists as a nonlinear term for the stimulated emission $gI(t)N(t)$. This nonlinearity is the origin of deterministic chaos and complex dynamics in lasers.

1.3.6 Relaxation oscillation frequency

The relaxation oscillation of the laser output intensity is one of the important characteristics to determine the frequency range of the temporal dynamics of lasers. Figure 1.14 shows a numerical example of relaxation oscillations in the intensity of a semiconductor laser when the device is turned on. The oscillations take place with a period that is considerably longer than the photon lifetime. The basic physical mechanism is the interplay between the laser intensity in the cavity and the population inversion. An increase in the laser intensity causes a reduction in the population inversion due to the increased rate of stimulated emission. This causes a reduction in the gain that tends to decrease the laser intensity. Then, the population inversion starts to increase again and the laser intensity follows the growth of the population inversion afterwards. This oscillatory behavior between the laser intensity and the population inversion continues for several cycles, and relaxes into stable values of the laser intensity and population inversion.

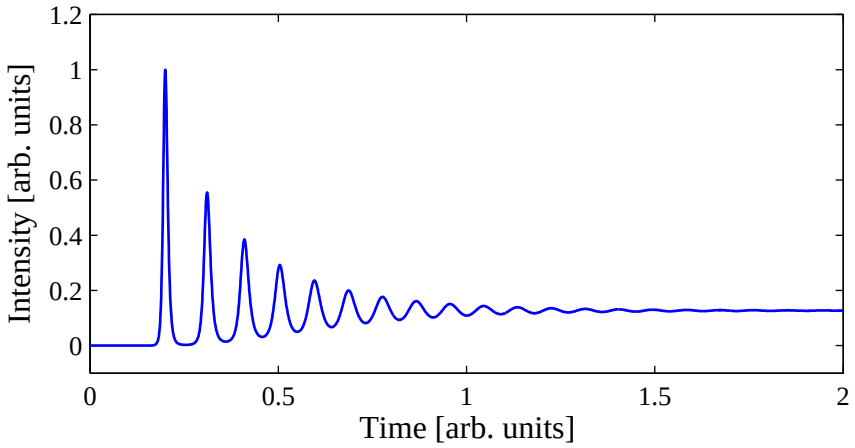

Figure 1.14: Numerical temporal waveform of the relaxation oscillations in the intensity of a semiconductor laser when the device is turned on. The model and the values of the parameters used in this example are the same as reference [17]

The relaxation oscillation frequency is dependent on the pump current, the carrier lifetime, and the photon lifetime in the laser cavity. Typical values of the relaxation oscillation frequency for different laser categories are summarized in Table 1.1.

	Population lifetime [s]	**Photon lifetime [s]**	**Relaxation oscillation frequency [Hz]**
Semiconductor lasers	10^{-9}	10^{-12}	$\sim 10^{9}$
Solid-state lasers	10^{-3}	10^{-9}	$\sim 10^{5}$
Gas lasers	10^{-8}	10^{-7}	$\sim 10^{6}$

Table 1.1: Relaxation oscillation frequencies for semiconductor, solid-state, and gas lasers [10, 18].

1.4 Chaos and lasers

In 1961, spontaneous irregular pulsations in the output intensity of the first laser were found by their inventors [8]. In that scientific paper, it was described that the amplitude of the individual pulses seen in the output intensity of the laser fluctuated in an "erratic manner". This description was the first historical observation of instabilities in a laser.

1.4.1 The "green" problem

Another example of instabilities in the output intensity of lasers can be found in the generation of green light (532 nm) from a diode-laser pumped Nd:YAG laser with an intracavity KTP potassium titanyl phosphate) crystal for second-harmonic generation, as shown in Figure 1.15(a) [19]. The Nd:YAG laser operates in a stable steady state emitting infrared radiation (1064 nm) without the intracavity crystal. When the intracavity KTP crystal is introduced, large intensity fluctuations are observed, as shown in Figure 1.15(b). It has been found that this occurs when the laser operates in several longitudinal modes. Sum-frequency generation in the KTP crystal can produce mode-mode coupling that destabilizes the laser output. The unstable behavior of this system has been known as the *green problem*.

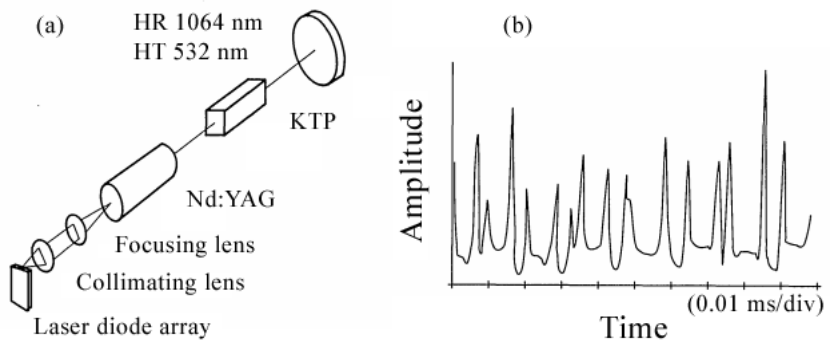

Figure 1.15: (a) Schematic diagram of a Nd:YAG laser with an intracavity-doubling crystal. (b) Irregular temporal waveform of the green laser output intensity (figure taken from reference [19]).

1.4.2 Connection between chaos and lasers

The ideas of both chaos and lasers were proposed in the early 1960s [4, 8]. The two research fields were developed independently, until Haken made the connection between lasers and chaos in 1975 [20]. He realized that the Maxwell-Bloch equations that describe the time evolution of the atoms and the electric field of a laser system and the Lorenz equations for the chaos model are isomorphic. The resulting differential equations are known as the Lorenz-Haken equations.

1.4.3 Classification of lasers based on decay rates

Lasers can be classified from the laser dynamics point of view [21]. The three relevant variables are the electric field, the atomic polarization, and the population

inversion. These variables usually decay on very different time scales, which are given by the electric field decay rate, the population inversion decay rate, and the atomic polarization decay rate. If one of these rates is larger than the others, the corresponding variable relaxes fast and consequently adiabatically adjusts to the other variables. In fact, because the temporal dynamics of the variable with large relaxation rate is faster than the other variables, this variable is regarded as a dependant variable when compared with the other ones and the number of equations describing the laser is reduced. This is known as *adiabatic elimination* of variables [10, 14]. According to the number of variables, lasers are classified into three types: class A, B, and C lasers.

1.4.3.1 Class C lasers (three variables)

For class C lasers, the decay rate of the electric field is comparable to those of the atomic polarization and the population inversion, thus, the dynamics of the three variables are described by 3 equations. Class C lasers satisfy the necessary condition for generating chaos (three independent variables). Examples of class C lasers are He-Ne lasers at the 3.39-μm line, He-Xe at the 3.51-μm line, and NH_3 lasers.

1.4.3.2 Class B lasers (two variables)

For class B lasers, the decay rate of the atomic polarization is much faster than those of the electric field and the population inversion, and the decay rate of the electric field is faster than that of the population inversion. The variable of the atomic polarization is regarded as a dependent variable and the dynamics of lasers is described by the two variables: the electric field and the population inversion. Class B lasers do not satisfy the condition for generation of chaos as they have only two variables. Class B lasers are stable in nature, but they are easily destabilized by external perturbations, resulting in the addition of extra degrees of freedom. Examples of class B lasers are semiconductor lasers, solid-state lasers, and CO_2 lasers.

1.4.3.3 Class A lasers (one variable)

For class A lasers, the decay rate of the electric field is much slower than those of the atomic polarization and the population inversion. The variables of atomic polarization and the population inversion change much faster than that of the electric field, and they are dependent on the electric field. In this case, only the variable of the electric field is used to describe the dynamics. Class A lasers are the most

stable lasers among the three classes, however, they may show chaotic behaviors by external perturbations with two or more extra degrees of freedom, as in the case of class B lasers. Examples of class A lasers are He-Ne lasers at the 632.8-nm line and dye lasers.

1.5 Semiconductor laser chaotic dynamics

Semiconductor lasers differ from conventional lasers not only in size, but also in "openness": while conventional lasers let escape only a small fraction of the light intensity to the outside world (1 - 5%) and are therefore considered "closed", semiconductor lasers are wide open, as they allow $\sim 70\%$ of the light intensity to escape. This goes two ways: semiconductor lasers are much more sensitive to perturbations from the "outside world" than other lasers. This difference causes semiconductor lasers to react strongly to external signals [14].

1.5.1 Chaos generation techniques

There are many techniques for generating chaos in semiconductor lasers with additional degrees of freedom. Three of them are: optical feedback, optical injection, and external modulation.

1.5.1.1 Optical feedback

In this technique, an external mirror is placed in front of the laser cavity, and the laser light is reflected back from the external mirror and reinjected into the laser cavity, as shown in Figure 1.16(a).

The reinjected optical signal from the same laser may disturb the balance of the carrier-photon interaction in the laser medium and induce the instability of the laser intensity. In this case, the temporal dynamics is determined by the two dominant frequency components: the relaxation oscillation frequency and the external cavity frequency. On the other hand, the external cavity frequency f_{ext} depends on the distance between the output facet of the laser cavity and the external mirror (i.e., the external cavity length) as

$$f_{ext} = \frac{c}{2nL_{ext}} , \tag{1.8}$$

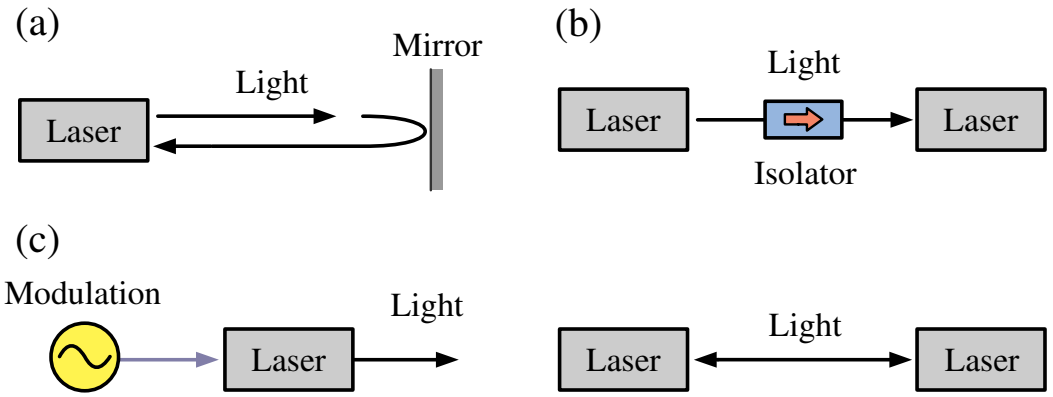

Figure 1.16: Three techniques for the generation of chaos in lasers with an additional degree of freedom: (a) optical feedback, (b) optical injection and coupling (upper: unidirectional coupling, lower: mutual or bidirectional coupling), (c) external modulation.

where L_{ext} is the external cavity length (one-way), n is the refractive index in the external cavity, and c is the speed of light. The external cavity frequency corresponds to the inverse of the round-trip time of light propagation in the external cavity.

1.5.1.2 Optical coupling and injection

The unidirectional or mutual optical coupling from one laser to another laser can generate chaotic instability of the laser output intensity, as shown in Figure 1.16(b). The laser intensity has two dominant frequency components. One is the optical-carrier frequency f_c determined by the optical wavelength λ and the speed of light c. f_c ranges in the order of several hundreds of THz (10^{14} Hz) for semiconductor lasers. The other frequency is the relaxation oscillation frequency f_r at the range of kHz - GHz (10^3 – 10^9 Hz). When the detuning of the optical carrier frequencies of both lasers is set to the order of the relaxation oscillation frequency, the nonlinear interaction between the optical-carrier frequency detuning and the relaxation oscillation frequency can occur and chaotic fluctuations may appear.

1.5.1.3 External modulation

When an external modulation is added to the pumping of a laser system, as shown in Figure 1.16(c), chaotic instability of the laser intensity may appear. The external modulation frequency needs to be set around the relaxation oscillation frequency of the laser, so that the nonlinear interaction between the external modulation frequency and the relaxation oscillation frequency may result in the generation of chaos.

The external modulation can also be applied to the loss of the laser cavity, which is referred to as *loss modulation*.

1.5.2 Low-frequency fluctuations

Low-frequency fluctuations (LFFs) are a type of chaotic oscillations observed in semiconductor lasers with optical feedback or injection under the conditions of low injection current and strong optical feedback. LFFs are characterized by sudden power dropouts followed by a gradual power recovery with a frequency that depends on laser parameters and the external cavity. The frequency of LFFs is of the order of MHz to a hundred MHz. Since the frequency of LFFs is much lower than ordinary chaotic fluctuations related to the relaxation oscillation frequency, the phenomena has been called low-frequency fluctuations. LFFs present a rich variety of dynamics. Figure 1.17 shows an example of an experimental low-frequency fluctuation waveform recorded with an oscilloscope.

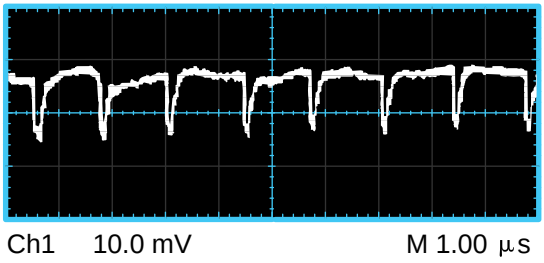

Figure 1.17: Experimental intensity time series of a semiconductor laser showing low-frequency fluctuations. The experimental setup is the same as the one that will be described in chapter 3, and the external cavity length is 9.0 m.

The power recovery is made in steps, not clearly visible in the figure because of the resolution of the oscilloscope used, and the duration of each step is equal to the round-trip time of light in the external cavity (around 40 ns for the example shown in Figure 1.17). LFFs have three components of different time scales. One is a low-frequency component with a period of microseconds; the second is a component related to the external cavity length with a period of tens of nanoseconds; the third is a high-frequency component related to the relaxation oscillations with a period of subnanoseconds (not visible in Figure 1.17 at that resolution).

1.5.3 Dynamics of semiconductor lasers with optical injection

A rich nonlinear dynamics can be observed in a semiconductor laser with optical injection from another laser (Figure 1.16(b)). In this scheme, light from a laser (referred to as the drive laser) is injected into the active layer of the another laser (the response laser). This configuration is often used to lock the optical-carrier frequency and stabilize the oscillation of a response laser, known as *injection locking*. Injection-locked semiconductor lasers are very useful for stabilizing the laser, however, they sometimes show a rich variety of dynamics outside the injection-locking range. Depending on the optical-carrier frequency detuning and the injection strength ratio, different regimes can be found, such as chaotic oscillations, low-frequency fluctuations, four-wave mixing, continuous-wave emission and bistability [10, 18, 22].

1.6 Synchronization of chaos

Christiaan Huygens was the first scientist who observed and described the synchronization phenomenon in the seventeenth century. He discovered that the oscillations of two pendulum clocks hanging from a common support coincided, and the pendula moved always in opposite directions. Huygens understood that the regularity of the rhythms of the two clocks was caused by an imperceptible motion of the common support, that is, the clocks were synchronized in anti-phase due to coupling through the support where both were hanging [23, 24].

After that initial discovery, many examples of synchronization in physical and biological systems have been found, and practical applications have been implemented. Some communication systems require synchronization of periodic carrier waveforms to tune an appropriate communication channel and extract an encoded message signal. Synchronization of periodic waveforms has been widely used in many engineering applications. In optics, injection locking between coupled lasers can be regarded as synchronization of periodic optical-carrier frequencies [10].

1.6.1 Synchronization of oscillatory systems

Synchronization is a phenomenon in which coupled dynamical systems present temporal oscillatory behaviors with a certain relationship [10]. This phenomenon is not only limited to systems that oscillate periodically; it can also be observed in coupled chaotic dynamical systems. Figure 1.18 shows an example of synchronization

of chaos. When the coupling strength is weak, two independent chaotic oscillations are observed, as shown in Figure 1.18(a).

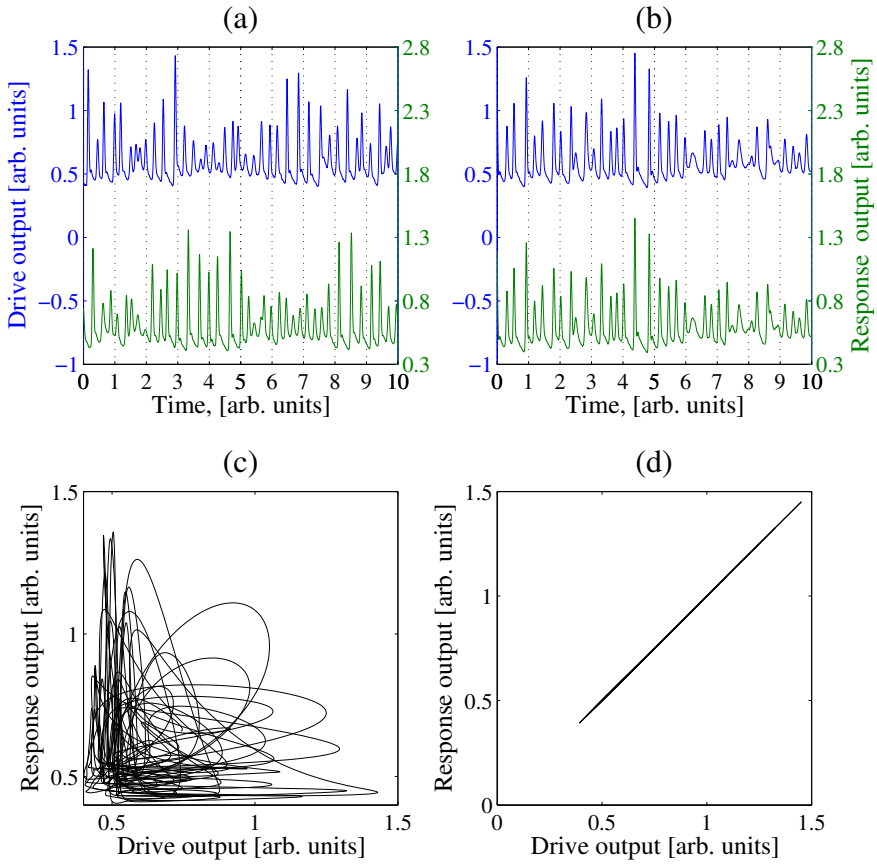

Figure 1.18: Examples of synchronization of (a), (b) chaotic temporal waveforms and (c), (d) corresponding correlation plots between the drive and the response systems. (a), (c) No synchronization. (b), (d) Synchronization of chaos.

When the coupling strength is increased, the two temporal waveforms start to show identical oscillations and synchronization of chaos can be achieved, as shown in Figure 1.18(b). The correlation plots, obtained from the temporal waveform of one oscillator versus that of the other coupled oscillator, show the appearance of synchronization between them (Figures 1.18(c), and (d)). There is no linear correlation between the chaotic temporal waveforms at weak coupling strength (Figure 1.18(c)). By contrast, a linear correlation is observed in Figure 1.18(d), showing identical synchronization of chaos (i.e., the systems evolve identically in time and their waveforms are in phase).

Several types of synchronization have been described in the literature, such as

identical (or *complete*) synchronization [25], *generalized* synchronization [26], *phase* synchronization [27], *lag* synchronization [28], and *anticipated* synchronization [29].

1.6.2 Oscillation death

In the middle of the nineteenth century, in his treatise called *The Theory of Sound*, William Strutt (better known as Lord Rayleigh) described an interesting phenomenon of synchronization in acoustical systems. Rayleigh observed mutual synchronization when two distinct but similar pipes began to sound at the same time, and also the effect of oscillation death (or quenching) when the coupling results in suppression of oscillations of interacting systems. [23].

Oscillation death is a particular case of synchronization in which, for sufficiently large coupling and frequency detuning between the oscillators, the oscillations in both systems may die out due to coupling. This phenomenon has been studied theoretically by several authors and demonstrated experimentally in many physical systems [30].

1.7 Multistability in lasers

Multistability or coexistence of different stable states (attractors) for a given set of parameters is an interesting phenomenon in dynamical systems that has been found in different fields, such as electronics, optics, mechanics, chemistry, biology, and economy [31]. The final state of a multistable system depends on the initial conditions. From the application point of view, this phenomenon can be undesirable, as is the case of the design of a commercial device with specific characteristics, where multistability needs to be avoided or the desired state has to be stabilized against a noisy environment. If the coexistence of multiple attractors is undesirable, control strategies to suppress multistability must be developed. On the other hand, the coexistence of different stable states offers a great flexibility if we consider that each attractor represents a different system performance.

During the last years, a lot of research has been performed to develop control techniques of multistable systems. These methods cover several strategies, going from feedback control methods to nonfeedback, such as periodic or stochastic perturbations capable of changing the coexisting states of stability and driving the system from multistability to monostability [31].

1.7.1 Multistability in optical systems

Multistability became an important phenomenon in laser physics in the beginning of the 80s, when it was shown experimental evidence of multistability in a modulated CO_2 laser [32]. Since then, multistability has been detected in other types of lasers, including a Nd:YAG laser with intracavity second harmonic generation, semiconductor, and fiber lasers.

The fast development of laser technology faces important technological problems which require multistability control. One famous example is the "green problem" [19] present in the operation of an intracavity frequency-doubled Nd:YAG laser. Usually, this laser emits infrared light, that can be converted into visible green light by using a nonlinear optical crystal. The nonlinear coupling between modes in the crystal gives rise to irregular fluctuations in the optical cavity. Such a behavior is attributed to the coexistence of multiple attractors which often appear in a system with many degrees of freedom. The irregularity in the laser intensity results from spontaneous switches between the coexisting states, so that additional stabilization mechanisms like a feedback control need to be applied to obtain a stable output. In modern fiber communication technology, semiconductor and fiber lasers are used to transmit a signal through a lightwave carrier. These lasers are nonlinear systems which can exhibit multistability when coupled to an external driving [33, 34]. This is another example, where multistability is undesirable because it affects communication efficiency and therefore it has to be avoided.

1.8 Noise-induced effects

As opposed to deterministic chaos, which obeys a deterministic rule that can be described by mathematical equations, noise is defined as an irregular temporal waveform generated from a stochastic process that is based on a statistical law. Irregular temporal waveforms of noise are not deterministic, and cannot be described by a set of nonlinear equations. Instead, the behavior of noise can be sometimes described by a set of differential equations driven by a sequence of random numbers as a stochastic term.

Most natural systems are intrinsically nonlinear and operate in noisy environments. Under certain circumstances, an extra dose of noise can in fact help rather than hinder the performance of some devices. Surprisingly, external noise can give rise to unexpected and interesting phenomena. For example, noise can change the stability properties of a system, namely stabilize or destabilize a steady state. Moreover, external noise can create new states that don't exist under deterministic envi-

ronmental conditions [35].

1.8.1 Stochastic resonance

The phenomenon of stochastic resonance appears when a nonlinear system operating in a noisy environment is driven by a periodic signal. At a certain noise amplitude the periodic response is maximal. The basic stochastic resonance mechanism can be intuitively understood by considering a simple system, like a bistable dynamical system that can switch between two stable states [36, 37], and supposing that the dynamics can be characterized by a potential function, as shown in Figure 1.19. The system can then be visualized as a marble inside a double well container. A gentle rocking of the container will cause the marble to roll back and forth within one of the wells; only under a much stronger disturbance will it surmount the wall and enter the other well. In the absence of any external forcing, friction will cause the system's output (the marble's position) to settle near the bottom of a well.

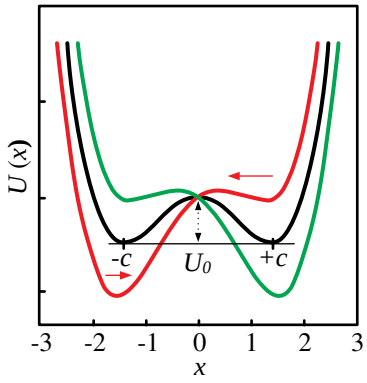

Figure 1.19: A bistable potential function (black line). In the absence of any forcing, the switching process between the two stable states (minima of the potential at $\pm c$) is driven by the noise; the escape rate across the potential "barrier", U_0, is the same in either direction. With a finite periodic forcing term added, the potential tilts periodically between the red and green configurations. When the periodic force is at its maximum (or minimum), the difference between the escape rates from the two states is maximum, as shown by the two unequal red arrows [36].

A more complex output is observed when an external forcing, composed of a deterministic signal and noise is applied. The external forcing may be interpreted as a periodic rocking of the potential, while is simultaneously moved randomly by the noise. The addition of even small amounts of noise can give a finite switching probability to the response; that is, some potential barrier crossings will occur. For moderate noise, the switching will acquire a degree of coherence with the underlying signal; the switching probability is maximized whenever the signal is at its own

maximum. The barrier-crossing rate thus depends critically on the noise intensity. If the noise intensity is very low, the probability of any switching is very small. On the other hand, intense noise can induce switching even during an interval when the signal is close to its minimum. In between, there are a range of noise intensities that induce switching events in near-synchrony with the signal.

The basic stochastic resonance effect is not limited to systems in which bistability occurs between two stable fixed points. Other forms of bistability (or multistability) abound in nature, and these systems can also display the same basic noise-enhanced response. A new generation of nonlinear devices and applications could use background fluctuations in a constructive way as an aid to performance, instead of considering them as something that always hinders performance and needs to be minimized. Stochastic resonance could find novel applications in physics, chemistry, biomedical sciences, and engineering.

1.8.2 Vibrational resonance

An analogous phenomenon to stochastic resonance, referred to as *vibrational resonance*, can occur when the noise is replaced by a high-frequency periodic signal. The phenomenon was discovered by studying a model where a high-frequency deterministic modulation replaced the added noise. It was numerically shown that the response to the periodic modulation (low frequency) in the absence of noise passes through a maximum, depending on the amplitude of an additional high-frequency modulation [38]. Experimental evidence and characterization of the phenomenon of vibrational resonance has been found in many different systems, such as electronic circuits [39], and optical systems [40]. This phenomenon could be applied to the detection of low-level signals, what could be a promising tool for a variety of applications such as signal restoring in optical fiber communication, optimization of threshold sensors in noisy environments, etc.

1.8.3 Coherence resonance

Another interesting noise-induced phenomenon is called coherence resonance. It resembles stochastic resonance, but has an important difference: while stochastic resonance appears if both periodic and noisy forces drive a nonlinear system, with the periodic response having a maximum at some noise amplitude, in coherence resonance, at some noise amplitude the regularity of the the noise-excited oscillations is maximal [41]. With stochastic resonance, noise can optimize a system's response to an external signal, while with coherence resonance, pure noise can generate the most coherent state in the system.

Chapter 2

Coherence enhanced intermittency

2.1 Abstract

In this chapter, we report on the experimental observation of coherence enhancement of noise-induced intermittency in a semiconductor laser subject to optical injection from another laser at the boundary of the frequency-locking regime. The intermittent switches between locked and unlocked states occur more regularly at a certain value of the injecting laser pump current. The probability distribution of the experimental inter-spike-interval fluctuations evaluated from the intensity time series is used to quantitatively characterize the intermittent behavior.

2.2 Introduction

Noise plays an important role in the dynamics of semiconductor lasers [42,43]. The intrinsic spontaneous emission noise is capable of exciting intensity multipulses from a steady state operation. Noisy lasers are known to exhibit self-pulsations in the locking region of optically injected semiconductor lasers [44]. Noise-induced excitability is related to the more general escape problem, where noise drives a system out of a potential well corresponding to a stable equilibrium over the potential barrier [45, 46]. Noise substantially modifies the dynamics near the locking between the injected field and the laser field; the noisy laser can produce pulses where the deterministic model allows for locking only.

Bistability in semiconductor laser injection locking was first experimentally demonstrated by Kawaguchi et al. [47] and then numerically simulated using different laser models [48,49]. The two stable states are associated with two different laser frequencies. One of them is the frequency of the injected light that captures the frequency of the injected laser, and the other one is the proper unlocked frequency of the injected laser. In the bistability domain at the boundary between frequency-locking and unlocked regimes, noise induces intermittent switches between the two coex-

isting steady states. The regularity of noise-induced spiking is a non-monotonic function of the spontaneous emission noise, and it is optimally correlated to a non-zero value of the noise intensity. This phenomenon referred to as coherence resonance [41, 50] was previously demonstrated theoretically and experimentally in a variety of dynamical systems, such as lasers with a saturable absorber [51], and lasers with optical feedback [52–54]. Recently, coherence resonance was predicted in the model of optically injected quantum-dot semiconductor lasers operated in the frequency-locked regime [49]. Experimentally it was shown that spontaneous emissions noise is sufficient to excite a semiconductor laser under optical injection operating in a stable locked continuous wave state close to the boundary of the frequency-locking regime [55]. Further, excitability and coherence resonance were experimentally observed in semiconductor lasers under optical feedback by adding broadband Gaussian white noise to the pump current [53, 54].

In this chapter, we will present experimental evidence of coherence enhancement in intermittent switches between two different laser wavelengths at the boundary of the frequency-locking regime in an optically injected semiconductor laser. We study how coherence can be enhanced by adjusting the injecting (master) laser pump current.

2.3 Experimental setup

The experimental setup is shown in Figure 2.1. We used two fiber-coupled discrete mode semiconductor lasers (Eblana Photonics) whose fiber ends were spliced to the rest of the fiber components by means of single-mode fiber. The lasers were stabilized in both the current and the temperature with accuracies of ± 0.01 mA and ± 0.01°C, respectively. An optical isolator (ISO) was inserted between the two lasers to provide unidirectional coupling between the master and slave semiconductor lasers, which were connected via two 90/10 fiber optical couplers (OC); 90% of the output radiation was used for the coupling through a polarization controller (PC) to ensure parallel polarization, and the remaining 10% was used for signal detection by photodetectors (PD) (Thorlabs PDB 150C, 150-MHz bandwidth). The signal from the photodetector was analyzed with an oscilloscope (Agilent Technologies DSO-X 3102A, 1-GHz bandwidth) and a frequency spectrum analyzer (FSA) (Agilent Technologies EXA N9010A, 9 kHz-13.6 GHz bandwidth). The laser wavelengths were monitored using an optical spectrum analyzer (OSA) (ANDO AQ-6315A). The threshold currents of the solitary master and slave semiconductor lasers are 11.5 mA and 12.0 mA at temperatures T = 20.0°C and T = 22.53°C, respectively. The injected power was regulated by an attenuator (Att). The wavelengths of both lasers were monitored with an optical spectrum analyzer (OSA) (ANDO AQ-6315A). The injected light of the master laser entered the optical spectrum analyzer after its

reflection at one of the components to the right of the second output coupler. Since the master laser was always in a continuous wave regime, the reflected light had no effect on temporal dynamics recorded by the oscilloscope.

The experimental data were acquired by means of the software LabVIEW 2012 through the equipment GPIB and USB ports.

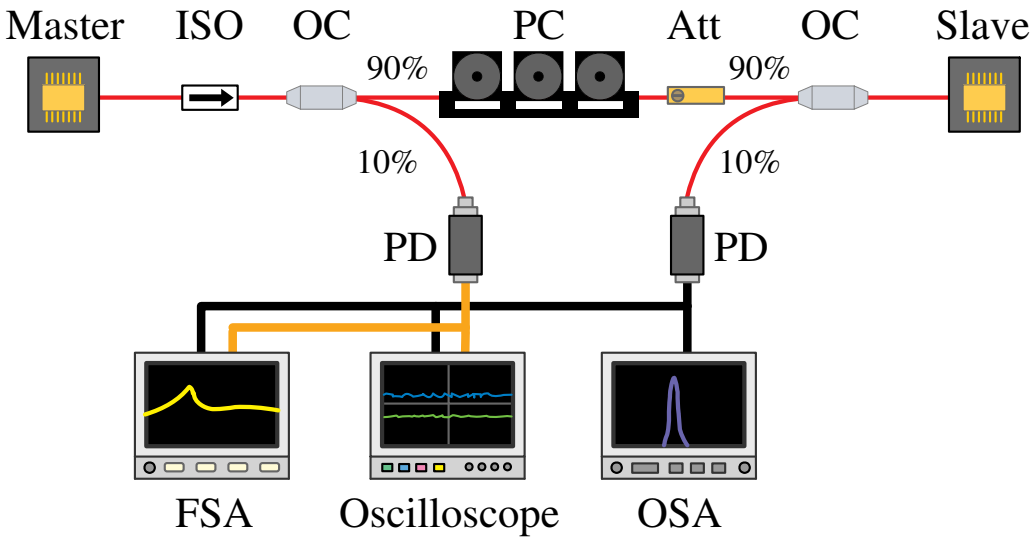

Figure 2.1: Experimental setup. PC: polarization controller, ISO: optical isolator, OC: output coupler, Att: optical attenuator, PD: photodetector, FSA: frequency spectrum analyzer, and OSA: optical spectrum analyzer. The red wire represents the single-mode optical fiber, and the black and yellow ones represent the electrical connections.

2.4 Time series and power spectra

During our experiments the slave laser driving current was fixed at $I_s = 12.80$ mA, and its temperature set at 22.5 °C. The master laser temperature was set at 20.0 °C and its pump current (I_m) was used as a control parameter. The selection of these values was made to allow the operation of both lasers at the same wavelength at some value of the control parameter. A change in (I_m) leads to approximately linear changes in both, laser power (Figure 2.2(a)) and wavelength (Figure 2.2(b)).

As we increased the master pump current from 0 mA, we observed that for 12 mA $< I_m <$ 22 mA the optical frequency of the slave laser was locked by the injected light, i.e. the slave laser emitted radiation at the same wavelength as the master laser since it started to lase. When I_m increased from 22 mA to 27 mA,

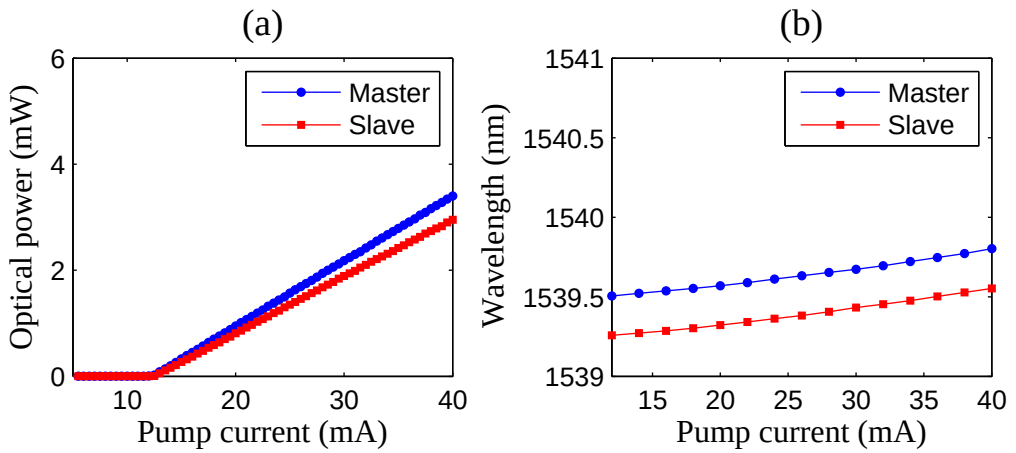

Figure 2.2: (a) Optical power as a function of the pump current for the solitary master and slave lasers. (b) Wavelength dependence of the pump current for both lasers. For the master laser T = 20.0 °C, and for the slave laser T = 22.5 °C.

the wavelength of the master laser increased from $\lambda_m = 1540.58$ nm to 1540.64 nm. Despite this slight increase, the slave laser dynamics changed drastically because the control parameter crossed the frequency-locking boundary, i.e. the system left the frequency-locking region and the injected light had no influence on the master laser anymore. This situation is illustrated in Figure 2.3 with the optical spectra and time series. At the boundary between the frequency-locking and unlocked regimes, the slave laser switched intermittently between the two wavelengths λ_m and λ_s, resulting in jumps between two different values of the slave laser intensity; the value with higher intensity corresponds to the frequency-locking regime and the lower intensity to the unlocked regime.

When 22 mA $< I_m <$ 24 mA the slave laser remained most of the time in the frequency-locking regime (higher intensity level), occasionally jumping to the unlocked state (lower intensity level), as seen in Figure 2.3(d,g). Around $I_m = 24.6$ mA the switches looked more regular with an average switching frequency of 3.7 MHz (Figure 2.3(e,h)). At $I_m = 25.4$ mA the slave laser remained most of the time in the unlocked state, presenting occasional switches to the locked state (Figure 2.3(f,i)).

For $I_m > 26.0$ mA the slave laser emitted again stable radiation being outside the frequency-locking region. Thus, the slave laser emission presented two well-defined stable states and the intermittency region between them. Such a behavior is illustrated in Figure 2.4 with the bifurcation diagram of the slave laser peak intensity. To obtain this diagram we analyzed 501 time series, each of a 1-ms long and comprised of 5×10^5 points, recorded for driving currents from $I_m = 18.00$ mA to 28.00 mA with a step of 0.02 mA. In Figure 2.4, one can clearly distinguish each

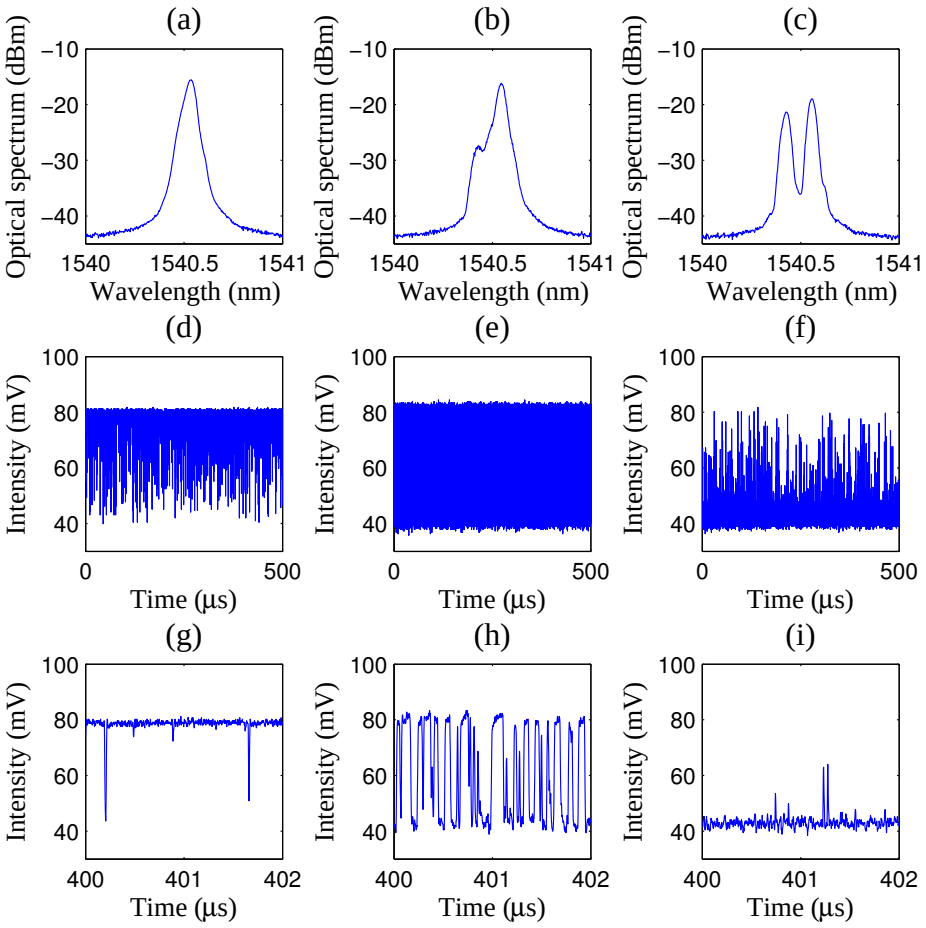

Figure 2.3: Average optical spectra recorded by OSA and oscilloscope time series for (a,d) $I_m = 22.0$ mA, (b,e) 24.6 mA, and (c,f) 25.4 mA. The lower row (g,h,i) shows a zoomed part of the above time series.

one of the two stable states and the intermittency region between 22.0 mA and 26.0 mA.

Figure 2.5 shows the evolution of the optical spectrum of both lasers recorded by the optical spectrum analyzer. Each one of the 1750 spectra (from $I_m = 5$ mA to $I_m = 40$ mA) is comprised of 1000 points. The color shows the power of the optical spectral components.

In Figure 2.5 we can see that, for small pump currents of the master laser ($I_m <$ 11.5 mA), i.e. below the laser threshold, only the wavelength of the slave laser ($\lambda_s \approx 1540.4$ nm) was present in the spectrum, and it was independent of I_m. At

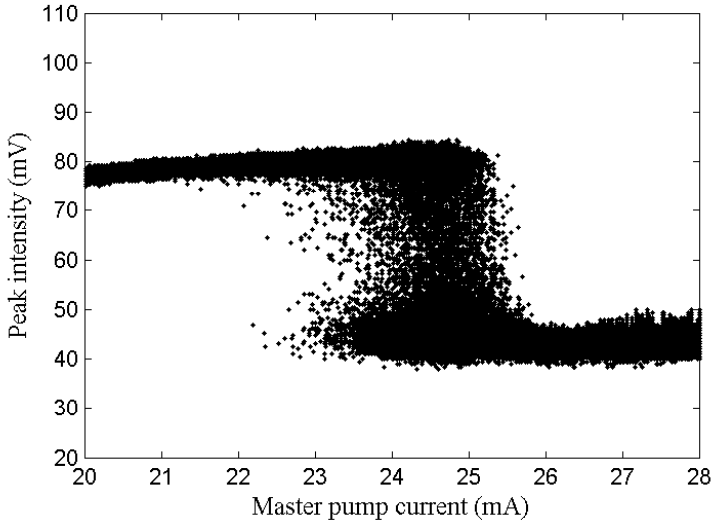

Figure 2.4: Bifurcation diagram of the slave laser peak intensity near the frequency-locking boundary.

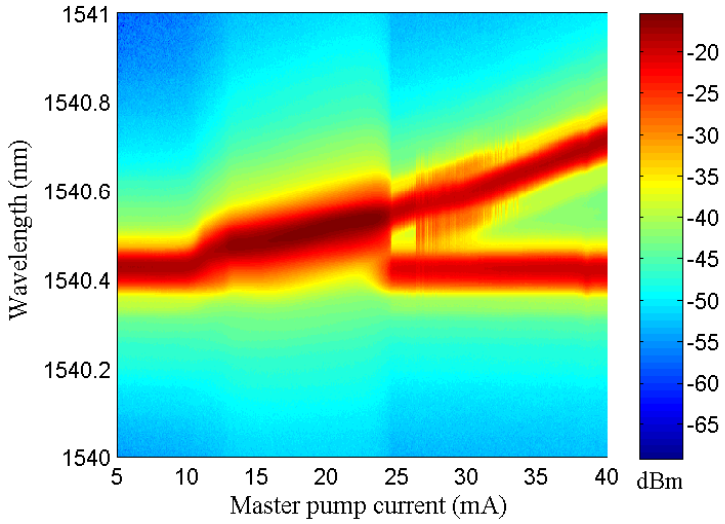

Figure 2.5: Bifurcation diagram of the optical spectral components at master and slave laser wavelengths.

$I_m = 11.5$ mA the master laser reached the lasing threshold and locked the slave laser frequency, i.e. $\lambda_s = \lambda_m$ for 12 mA $< I_m <$ 21 mA. For larger currents (21 mA $< I_m <$ 26 mA) the slave laser exhibited an intermittent behavior. When the difference between λ_s and λ_m was smaller than the optical spectrum analyzer spectral resolution ($\pm$ 0.05 nm), the local maximum at λ_s did not appear in the optical spectrum. This results in the approximately 0.05-nm width of the lines in

the diagram. When the separation between the lines corresponding to the master and slave laser wavelengths was large enough, we were able to distinguish two peaks in the spectrum, as in Figure 2.3(b). If not [as in Figure 2.3(a)], we could only decide that the laser switched between the two wavelengths by observing the time series recorded with the oscilloscope. Finally, for $I_m > 26$ mA each laser emitted at its own free-running frequency. For high currents, the two lines in Figure 2.5 represent two independent wavelengths, the upper one corresponds to λ_m, which increases with I_m, and the lower one, fixed at 1540.4 nm, corresponds to the free-running frequency of the slave laser.

To test the reproducibility of these bifurcation diagrams, we performed the measurements many times and we obtained the same behavior. The injected power was too small to induce chaos in the slave laser, what makes us believe that the spiking and switching dynamics at the frequency-locking boundary has a stochastic origin due to internal noise.

2.5 Coherence enhancement

The observed intermittency is known to be induced by noise inherent to semiconductor lasers [49]. The noisy behavior of the laser emission is clearly seen in Figure 2.4 as a broaden width of the upper and lower branches of the bifurcation diagram. In the bistability domain, the system behavior can be presented in the form of a double-well potential with a current-dependent shape. Unlike coherence resonance which is characterized by increasing regularity with respect to noise, in our case the noise is almost constant and the regularity is optimized for a certain value of the master laser current when the double-well potential is more symmetric. On-off intermittency is typically defined by conditions for the onset of intermittent behavior, namely, the distribution of laminar phases and the mean laminar phase versus a control parameter, usually noise intensity [56]. Since our laser displays either separate spikes, like those in Figures 2.3(g) and 2.3(i), or switches between two equilibrium states, like those in Figure 2.3(h), it is not possible to measure the duration of the turbulent phase and hence characterize this type of intermittency by commonly used scaling relations. Therefore, similar to neuron systems, we measure inter-spike-intervals (ISI) between consecutive optical spikes or switches, evaluated by $\Delta T_i = t_{i+1} - t_i$, with t_i being the time when a spike occurs. The inter-spike-interval fluctuations are defined as the difference between the natural logarithms of successive inter-spike-intervals

$$\Delta_n = \ln(\Delta T_{i+1}) - \ln(\Delta T_i) \, . \tag{2.1}$$

To find Δ_n in the intermittency region of our system, we analyzed the time series and measured ΔT_i as the spike amplitude crossed the value of 60 mV (Figure 2.6). This threshold was selected because it lies at the middle of the two system states. For spikes whose amplitude did not cross the value of 60 mV, ΔT_i was calculated as the distance between the consecutive local minima or local maxima.

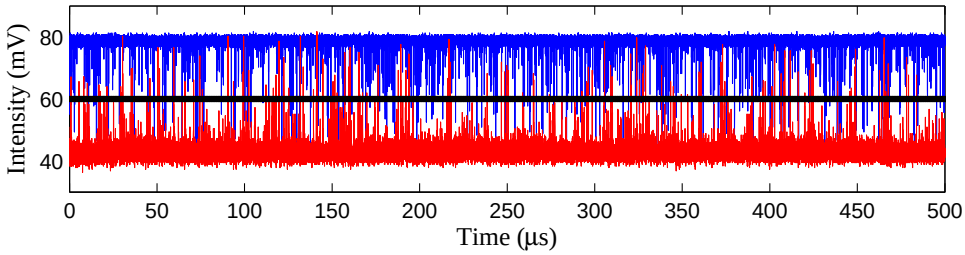

Figure 2.6: Time series for $I_m = 22.0$ mA (blue trace) showing the jumps to the lower intensity level, and for $I_m = 25.4$ mA (red trace) showing the jumps to the locked state. The horizontal line represents the 60 mV threshold for the determination of the spikes in the time series.

The current dependence of the standard deviation (SD) of Δ_n in the intermittency region, shown in Figure 2.7(a), displays a minimum around 24.5 mA, meaning that the system dynamics exhibits maximum coherence.

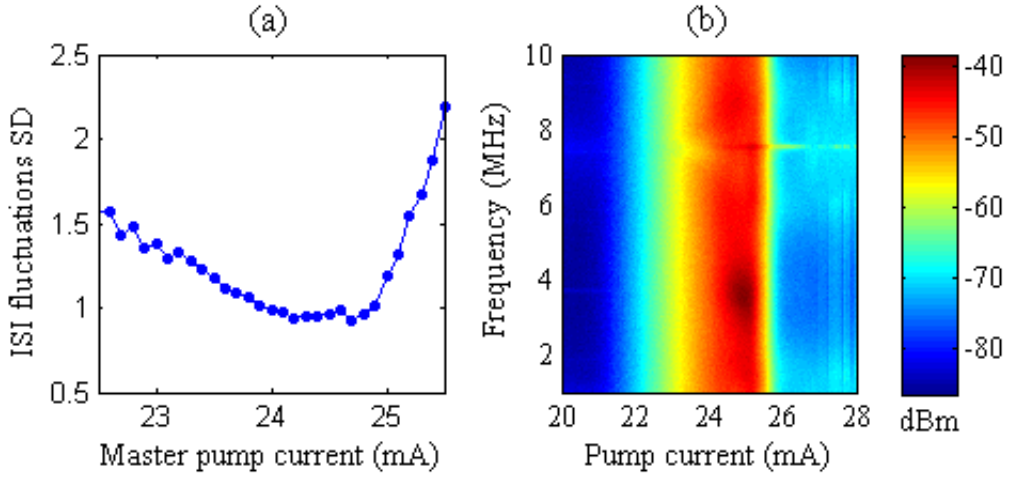

Figure 2.7: (a) Standard deviation of inter-spike-interval fluctuations in the intermittency region, and (b) power spectrum as a function of the master laser pump current. The minimum in (a) and the dark spot in (b) correspond to maximum coherence.

The asymmetry in the curve has a relation with the density of points in the boundaries of the intermittency region observed in the bifurcation diagram shown

in Figure 2.4. The transition from the higher intensity level to the lower one is more gradual at the beginning than at the end, where it finishes more abruptly. This could have an effect in the slope of the curve before and after the minimum around 24.5 mA.

It should be noted that small variations in the amplitude threshold do not produce qualitative changes in Δ_n.

Another quantitative measure of the coherence is the power of the dominant spectral component in the frequency spectrum. The higher the power at a particular frequency, the more regular dynamics is. Figure 2.7(b) shows the power spectrum as a function of I_m. The dark spot in the vicinity of 25 mA means that the laser behavior for this pump current is more regular than for other currents, because of the existence of the dominant frequency of about 3.7 MHz at which the power was significantly higher than for other spectral components. Another, but no so pronounced maximum occurred at the second harmonic of this frequency.

Next, we show that the fluctuations presented by this system can be fitted by non-Gaussian stable distributions. Stable distributions are a class of probability distributions that allow skewness and heavy tails, i.e. tails that are "heavier" than an exponential decay. This means that events, which are far from the average, appear more frequently than in the Gaussian case (Figure 2.8).

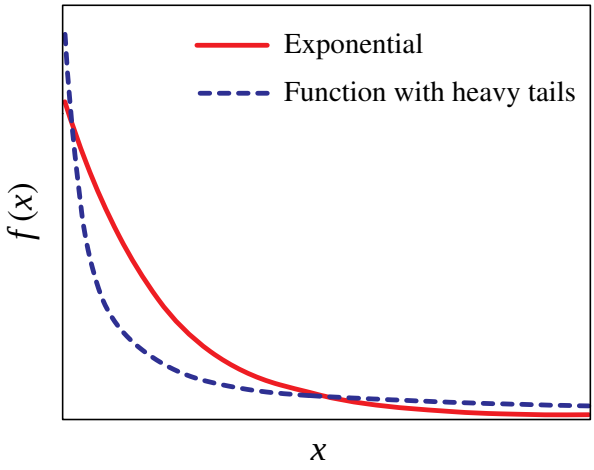

Figure 2.8: Comparison between an exponentially decreasing function (solid red trace) and a heavy-tailed function (dashed blue trace). For values of x far from the origin, the heavy-tailed function has values that are bigger than the exponential function.

One argument for modeling a system with stable distributions is empirical: many large data sets exhibit heavy tails and skewness. Some data sets from many fields are poorly described by a Gaussian model, but can be well described by a stable

distribution [57]. Heavy tailed distributions have been found in different areas, from economics and finance to engineering and biology [57–60].

Before presenting the mathematical expression for non-Gaussian stable distributions, the concept of *stable* will be defined (a detailed description of stable distributions can be found in reference [57]). An important property of normal or Gaussian random variables is that the sum of two of them is itself a normal random variable. One consequence of this is that if X is normal, then for X_1 and X_2 independent copies of X and any positive constants a and b

$$aX_1 + bX_2 \stackrel{d}{=} cX + d \,, \tag{2.2}$$

for some positive c and some $d \in \mathbb{R}$. The symbol $\stackrel{d}{=}$ means equality in distribution, i.e. both expressions have the same probability law. Equation (2.2) says that the shape of X is preserved (up to scale and shift) under addition. A random variable X is stable if for X_1 and X_2 independent copies of X and any positive constants a and b, Equation (2.2) holds for some positive c and some $d \in \mathbb{R}$. The word *stable* is used because the shape is stable or unchanged under sums of the type represented by Equation (2.2) [57].

There are three cases where it is possible to write down closed form expressions for the probability density and it can be verified that they are stable: Gaussian, Cauchy and Levy distributions. For the normal or Gaussian distributions, the probability density can be expressed as

$$f(x) = \frac{1}{\sqrt{2\pi}\sigma} \exp\left(-\frac{(x-\mu)^2}{2\sigma^2}\right) \,, \; -\infty < x < \infty \,, \tag{2.3}$$

where μ is the mean and σ is the standard deviation. For the Cauchy distributions, the probability density can be expressed as

$$f(x) = \frac{1}{\pi} \frac{\gamma}{\gamma^2 + (x-\delta)^2} \,, \; -\infty < x < \infty \,, \tag{2.4}$$

For the Lévy distributions, the probability density can be expressed as

$$f(x) = \sqrt{\frac{\gamma}{2\pi}} \frac{1}{(x-\delta)^{3/2}} \exp\left(-\frac{\gamma}{2(x-\delta)}\right) \,, \; \delta < x < \infty \,. \tag{2.5}$$

Gaussian and Cauchy distributions are symmetric bell-shaped curves. The main qualitative distinction between them is that the Cauchy distribution has much heavier tails. In contrast to the Gaussian and Cauchy distributions, the Levy distribution is highly skewed, with all of the probability concentrated on $x > 0$, and it has even heavier tails than the Cauchy. General stable distributions allow for varying degrees of tail heaviness and varying degrees of skewness.

There are other equivalent definitions of stable random variables that will help to present the general form of stable distributions.

Definition 2.1 X is stable if and only if for all $n > 1$, there exist constants $c_n > 0$ and $d_n \in \mathbb{R}$ such that

$$X_1 + \cdots + X_n \stackrel{d}{=} c_n X + d_n \ , \tag{2.6}$$

where $X_1, \ldots, X_n$ are independent, identical copies of X. It can be shown that the only possible choice for the scaling constants is $c_n = n^{1/\alpha}$ for $\alpha \in (0, 2]$. While useful, these conditions do not give a concrete way of parameterizing stable distributions. The most concrete way to describe all possible stable distributions is through the characteristic function or Fourier transform (for a random variable X with distribution function $F(x)$, the characteristic function is defined by $\phi(u) = E \exp(iuX) = \int_{-\infty}^{\infty} \exp(iux) dF(x)$. The function $\phi(u)$ completely determines the distribution of X).

Definition 2.2 A random variable X is *stable* if and only if $X \stackrel{d}{=} aZ + b$, where $0 < \alpha \leq 2$, $-1 \leq \beta \leq 1$, $a \neq 0$, $b \in \mathbb{R}$ and Z is a random variable with characteristic function

$$E \exp(iuZ) = \begin{cases} \exp(-|u|^{\alpha}[1 - i\beta \tan \frac{\pi\alpha}{2}(\text{sign}(u))]), & \alpha \neq 1 \\ \exp(-|u|[1 + i\beta \frac{2}{\pi}(\text{sign}(u)) \log |u|]), & \alpha = 1 \end{cases} . \tag{2.7}$$

These distributions are symmetric around zero when $\beta = 0$ and $b = 0$. General stable distributions require then four parameters: an index of stability or characteristic exponent $\alpha \in (0, 2]$, a skewness parameter $\beta \in [-1, 1]$, a scale parameter $\gamma \geq 0$, and a location parameter δ. The parameter α is an indicator of the tails. For $\alpha = 2$ the distribution is Gaussian, and smaller values imply heavier tails. For $\beta = 0$ the distribution is symmetric, and a different value means that the distribution is skewed either to the left or to the right, depending on the sign. The parameter γ is an indicator of the distribution width. The parameter δ moves the distribution horizontally, depending on its value. Since α and β determine the distribution form,

they are considered shape parameters.

There are multiple parametrizations for stable laws, and some are more suitable in certain situations. The variety of parametrizations is due to a combination of historical evolution, plus the numerous problems that have been analyzed using specialized forms of the stable distributions. In the notation $\mathbf{S}(\alpha, \beta, \gamma, \delta; k)$, the integer k indicates the parametrization. The recommended parametrization for numerical work and statistical inference with stable distributions is $\mathbf{S}(\alpha, \beta, \gamma, \delta; 0)$ (S0 for short) because it has the simplest form for the characteristic function that is continuous in all parameters.

Definition 2.3 A random variable X is $\mathbf{S}(\alpha, \beta, \gamma, \delta; 0)$ if

$$X \stackrel{d}{=} \begin{cases} \gamma(Z - \beta \tan \frac{\pi\alpha}{2}) + \delta, & \alpha \neq 1 \\ \gamma Z + \delta, & \alpha = 1 \end{cases}, \tag{2.8}$$

where $Z = Z(\alpha, \beta)$ is given by Equation (2.7). X has characteristic function

$$E \exp(iuX) = \begin{cases} \exp(-\gamma^\alpha |u|^\alpha [1 + i\beta \tan \frac{\pi\alpha}{2} (\text{sign}(u))(|\gamma u|^{1-\alpha} - 1)] + i\delta u), & \alpha \neq 1 \\ \exp(-\gamma |u| [1 + i\beta \frac{2}{\pi} (\text{sign}(u) \log(\gamma |u|)] + i\delta u), & \alpha = 1 \end{cases}. \tag{2.9}$$

The above expression defines the general stable law in the S0 parametrization. The fitted stable parameters of this kind of probability distributions are showing to be a useful tool to quantify and monitor the state of complex systems.

To fit the inter-spike-interval fluctuations we used the computer program called *Stable*, which performs an estimation of the stable parameters [61, 62]. Depending on the problem to be solved, a particular parametrization could be used. In the Stable program, all computations are performed in the S0 parametrization, which is better suited to numerical calculations and modeling data.

Figure 2.9 shows an example of stable probability densities in the S0 parametrization for two different values of the characteristic exponent: (a) $\alpha = 2$, and (b) $\alpha = 1$. Skewness is indicated by the trace color: $\beta = 0$ (black), $\beta = 0.25$ (red), $\beta = 0.5$ (green), $\beta = 0.75$ (yellow), $\beta = 1$ (blue). In all cases, the scale parameter $\gamma = 1$ and the location parameter $\delta = 0$. [61, 62]. Figure 2.9(a) shows that, for $\alpha = 2$ (the Gaussian case), the value of the skewness parameter has no effect on the shape of the distribution and all the curves are superimposed. Figure 2.9(b) shows that, for a smaller value of the characteristic exponent, the distributions have heavier tails and the skewness parameter value has an evident effect in the distribution shape.

For smaller values of α, these two effects increase.

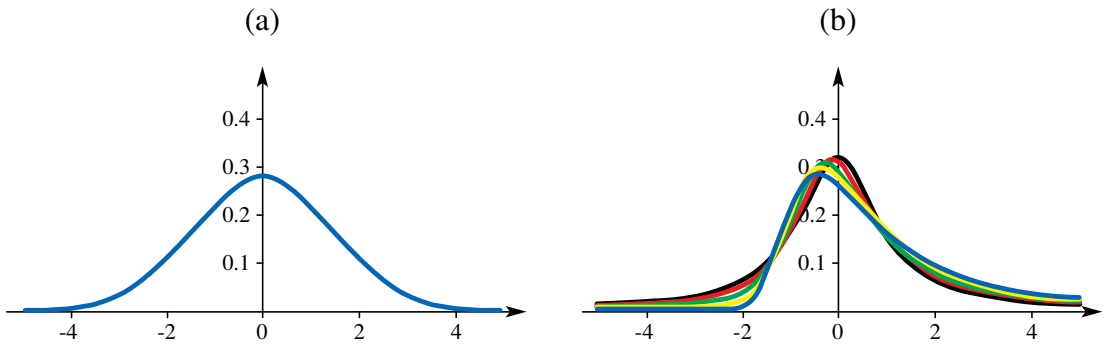

Figure 2.9: Stable probability densities in the S0 parametrization for two different values of the characteristic exponent: (a) $\alpha = 2$, and (b) $\alpha = 1$. Skewness is indicated by the trace color: $\beta = 0$ (black), $\beta = 0.25$ (red), $\beta = 0.5$ (green), $\beta = 0.75$ (yellow), $\beta = 1$ (blue). In all cases, the scale parameter $\gamma = 1$ and the location parameter $\delta = 0$. [61, 62].

In the Stable program, the probability density, obtained with a Gaussian kernel for the experimental data is compared with the fitted stable probability density. The stable model is acceptable if there is a good agreement between the fitted stable density and the data density, and if the variance-stabilized PP (percent-percent) plot of the data versus the fit is essentially on a 45-degree line [63]. We found that the smoothed data density of the experimental inter-spike-interval fluctuations was in good agreement with the fitted stable density, and that the PP plot of the data versus the fit was on a 45-degree line for the range of pump currents in the intermittency region, as shown in Figure 2.10(a), and 2.10(b).

The stable fitted parameters α and γ in the intermittency region plotted with the 95% confidence interval are shown in Figure 2.11. We can see that at the center of the intermittency region α is very close to 2 ($\alpha = 1.99$), and before and after this region the characteristic exponent is around 1.9. For $\alpha = 2$, the parameter β has no effect on the shape of the distribution [57].

The parameter γ represents the same behavior as the standard deviation of the inter-spike-interval fluctuations, since it is related with how spread the distribution is. On the other hand, the parameter δ was practically zero for all pump currents.

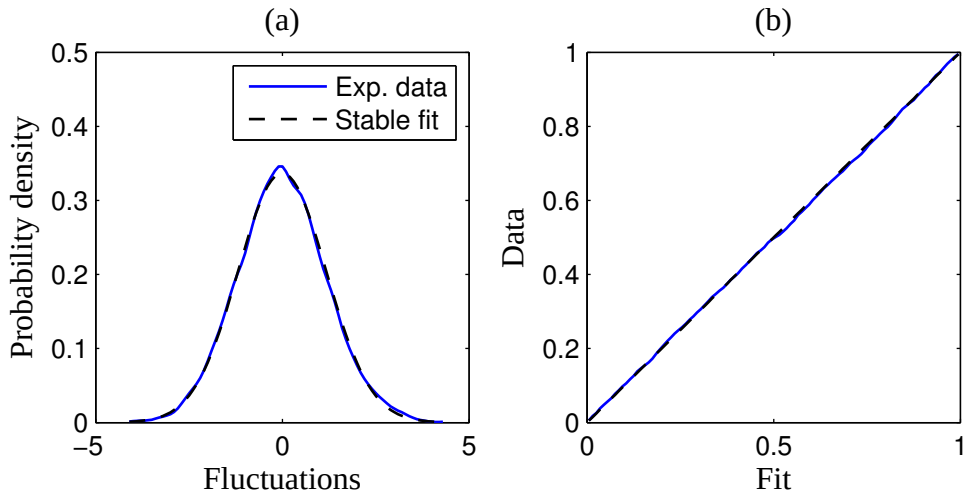

Figure 2.10: (a) Fitted stable and data probability densities, and (b) variance-stabilized PP plot when the pumping current is 24.6 mA. A 45-degree dashed line was drawn as a reference.

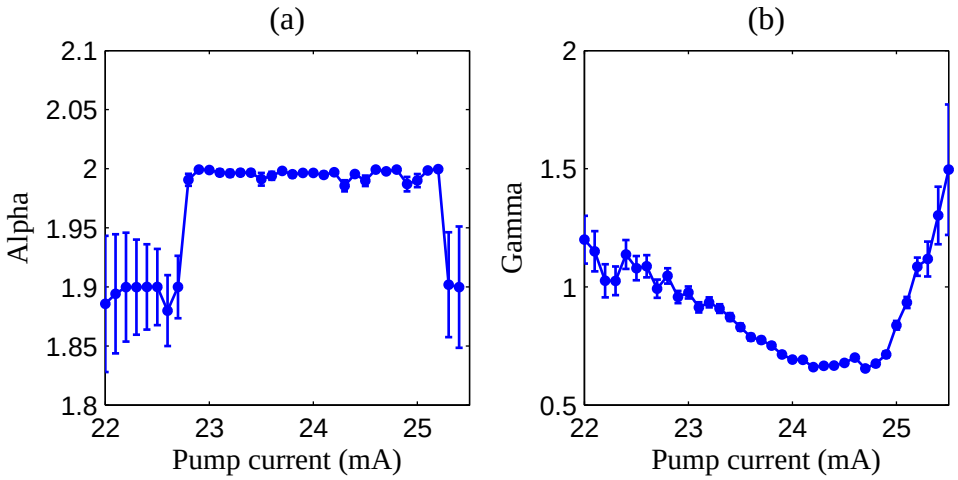

Figure 2.11: Fitted stable parameters (a) α and (b) γ as a function of the master laser pump current. The 95% confidence intervals are plotted.

2.6 Conclusion

In this work we have presented experimental evidence of coherence enhancement of noise-induced intermittency in an optically injected semiconductor laser at the boundary of the frequency-locking regime. With the bifurcation diagrams of the laser peak intensity and the optical spectral components we have shown the exis-

tence of intermittent switches between the frequency-locking and unlocked regimes. The minimum in the standard deviation of the inter-spike-interval fluctuations has indicated the existence of the optimal master laser pump current for highest coherence of the intermittent jumps. Furthermore, the power spectrum exhibited the prevalence of a particular spectral component or the existence of a dominant frequency. We have associated this phenomenon with an improvement in the symmetry of the double-well potential. We have also found that the inter-spike-interval fluctuations in the intermittency regime obeyed two different probability distributions, a non-Gaussian stable distribution (heavy tailed) for the spiking behavior near one equilibrium state, and a normal distribution for the random switches between the two states, quantified by fitted stable parameters α and γ. The stable fit can be used to select adequate models and parameters for simulating intermittent dynamics by comparing the fitted stable parameters obtained from experimental and numerical data.

Chapter 3

Noise-induced intermittency

3.1 Abstract

In this chapter, we report on the experimental observation of intermittent switches between low-frequency fluctuations and steady-state emission in two bidirectionally coupled semiconductor lasers subject to common Gaussian noise applied to their laser pump currents. The time series analysis revealed power-law scalings typical for on–off intermittency near its onset, with critical exponents of -1 for the mean turbulent length versus noise intensity and -3/2 for the probability distribution of laminar phases versus the laminar length. Moreover, the same -1 power-law scaling was also found by the power spectrum analysis for the signal-to-noise ratio versus the noise intensity.

3.2 Introduction

In the 1970s, some researchers observed an intermittent transition to turbulence in experiments made in Rayleigh-Bénard cells using fluids. In these experiments, the temperature difference between the bottom and the top of a cell containing the fluid was selected as a control parameter (Figure 3.1).

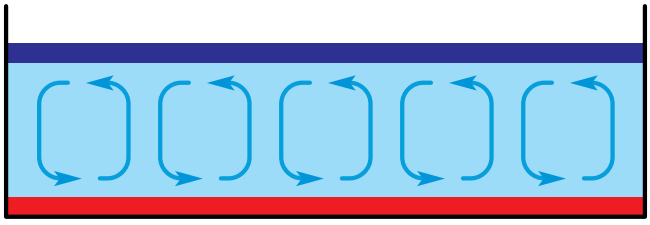

Figure 3.1: Schematic representation of a Rayleigh-Bénard cell. The fluid is confined between plates held at constant temperature. The hot plate is below and the cold one above.

Below a critical value of this parameter, the fluid moved following periodic oscillations. Just above the critical value of this parameter, the fluid remained apparently in a periodic state during long time intervals, but this regular behavior seemed to be randomly and abruptly disrupted by a "burst" of finite duration. After that sudden burst, a new laminar phase started, and so on. As the control parameter was increased, it became more and more difficult and finally impossible to recognize the regular oscillations. In 1980, Yves Pomeau and Paul Manneville studied this problem mathematically and introduced the term "laminar phase" to refer to the time intervals in which the fluid remained in a regular state (the bursts were later called the "turbulent phase"). Since then, this terminology has been used when intermittency is found in a nonlinear dynamical system. Pomeau and Manneville showed that this sort of transition to turbulence is also present in simple dissipative dynamical systems, such as the Lorenz model, and they classified intermittency in three types: *type I* is associated with an inverse tangent bifurcation, *type II* with a Hopf bifurcation, and *type III* with a period-doubling bifurcation [64]. Besides the three types of the Pomeau-Manneville intermittency, two more types were later discovered: *crisis-induced intermittency* [65] and *on-off intermittency* [66]. Intermittency is a phenomenon that is not only limited to fluids; it is a behavior that nonlinear dynamical systems can exhibit, and is one of the routes from a regular state to a chaotic motion that a system can undergo.

The phenomenon of intermittency occurs when a system passes through a critical point. For example, type I and on–off intermittency are related with saddle-node bifurcations, type II and type III with Hopf and inverse period-doubling bifurcations, respectively, and crisis-induced intermittency with a crisis of chaotic attractors.

Qualitatively and quantitatively, all kinds of intermittency are different. Qualitatively, the mechanism for on-off intermittency requires a time-dependent modulation of a bifurcation parameter through a bifurcation point; in Pomeau-Manneville and crisis-induced intermittency the parameters are fixed. Quantitatively, every kind of intermittency exhibit a characteristic interbust interval (laminar phase) statistics.

A distinctive feature of on–off intermittency is that the system's parameter modulation has to be either random, chaotic, or periodic [56, 65–69]. In on–off intermittency, one or more dynamical variables exhibit two distinct states as the system evolves in time. In the "off" state (the laminar phase), there are various time intervals where the variables remain approximately constant, whereas in the "on" state (the turbulent phase), irregular bursts of the variables away from their constant values occur. On–off intermittency is characterized by two fundamental statistical properties: power-law scalings near the onset of intermittency have -1 critical exponents for the mean duration of the laminar phase versus a control parameter and -3/2 for the probability distribution of the laminar phases versus the laminar length [56].

Next, we will briefly summarize the main quantitative characteristics of on-off intemittency. A deep treatment can be found in reference [56]. The essential features of on-off intermittency were first described in the context of one-dimensional parametrically driven maps, where on-off intermittency was achieved with random and chaotic parameter variations. The maps studied were of the form

$$y_{n+1} = z_n f(y_n) \ , \tag{3.1}$$

where $f(0) = 0$, $\partial f(y)/\partial y \mid_0 \neq 0$, and the variable z_n represents a random or a chaotic process.

An example of this family of maps can be produced if $f(y_n) = y_n(1-y_n)$ and $z_n = ax_n$, where x_n is a random variable in the interval $[0, 1]$ with uniform distribution and $a > 1$. In this case, the map described by Equation (3.1) is a logistic map with a random parameter. For $a = 2.8$, the time series displays long periods of nearly constant signal interrupted short periods of larger amplitude bursts. The type of intermittency observed is different from Pomeau-Manneville type-I, -II, and -III intermittency, as well as crisis induced intermittency. These types of intermittency occur for fixed values of the bifurcation parameter, while the bifurcation parameter in on-off intermittency is a dynamical variable.

The major features for the map described by Equation (3.1) are

1. For $a < e$, the signal y_n decays to zero.
2. For $a \geq e$, the time series of y_n present a sustained intermittent behavior, displaying long periods near $y = 0$ (the laminar phases) and short periods of large amplitude bursts (the turbulent phase). $a = e$ is the threshold for intermittent behavior to occur.
3. For $a \geq e$ and $a \approx e$ (the onset of intermittency), the probability distribution Λ_n of laminar phases obeys a power law scaling of the form $\Lambda_n \sim n^{-3/2}$, where n is the length of the laminar phase. This universal feature holds for a large class of driving processes x_n.
4. Beyond the onset, the distribution of laminar phases decreases exponentially with n as $n \to \infty$.
5. Near the onset ($a = e$), the mean laminar phase obeys a power law with critical exponent = -1 of the form $\langle n \rangle \approx \delta^{-1}$, where $\delta = a - e$ is the distance from the onset parameter.
6. Nonlinearity is essential for sustaining the intermittent behavior, but an instability is the source of the intermittent bursts.

Even though these results are based on the dynamics of a class of one-dimensional maps, the scaling relations for on-off intermittency have been experimentally proven in a wide variety of systems, which include electronic circuits [70,71], a gas discharge plasma [72], nematic liquid crystals [73, 74], synthetic dynamos [75], a human balancing task [76], a distributed-feedback semiconductor laser [77], a diode laser with external cavity [68], and an optically injected dual-mode semiconductor laser [48].

To distinguish between the different kinds of intermittency in experiments, it is necessary to analyze the measured properties (the distribution of laminar phases and the average laminar phase) and to identify the mechanism for the intermittent behavior. For instance, type-III intermittency has the same scaling laws as on-off intermittency. However, in type-III intermittency the intermittent signals exhibit bursts about either side of the fixed point. Type-I and type-II intermittency have power-law laminar phase distributions with critical exponents -1/2 and -2, respectively, and their mean laminar phases scales as $\delta^{-1/2}$ and δ^{-1}, respectively. Finally, the laminar phases in crisis-induced intermittency are segments of chaotic orbits representing jumps between former separate attractors. In contrast, the laminar phases in on-off intermittency are nonchaotic (fixed points or periodic orbits) [56, 66].

In this chapter, we report on noise-induced intermittency between coexisting regimes of low-frequency fluctuations and a continuous wave emission in almost identical mutually delay-coupled semiconductor lasers under the influence of external Gaussian noise. We associate this phenomenon with on–off intermittency characterized by their particular scaling laws. The interest in the dynamics of delay-coupled semiconductor lasers arises from its usefulness for both technical applications and fundamental research. The understanding of the dynamical behavior of semiconductor lasers is highly important for advancing technology in optical communication using a chaotic carrier [78]. On the other hand, these lasers are canonical systems for studying general properties of delay-coupled oscillators which occur in many areas of science and in nature [79], for example, neural networks [80], chemical reactors [81], and electronic circuits [82]. Delay-induced bistability, namely, the coexistence of low-frequency fluctuations and stable continuous wave emission has been observed in a semiconductor laser with delayed optical feedback [83–85], and noise-induced alternation between low-frequency fluctuations and continuous wave has been detected [77, 85]. Although the dynamics of mutually coupled semiconductor lasers has been investigated [22, 86, 87], only few works are related to the effects of noise in these lasers [22].

3.3 Experimental setup

The experiments were performed with two fiber-coupled discrete mode semiconductor lasers (Eblana Photonics, 1542 nm), and their currents and temperatures were stabilized with accuracies of $\pm$ 0.01°C and 0.01 mA, respectively. As shown schematically in Figure 3.2, the lasers were connected via 90/10 fiber beam-splitters; 90% of the output radiation was used for the coupling through a polarization controller (PC) to ensure parallel polarization and the remaining 10% was used for detection by InGaAs PIN photodetectors (Thorlabs PDA8GS, 9.5-GHz bandwidth). The signals from the photodetectors were analyzed with a frequency spectrum analyzer (Agilent Technologies EXA N9010A, 9 kHz–13.6 GHz bandwidth) and an oscilloscope (Tektronix TDS520, 500-MHz bandwidth). The optical spectra was measured with an optical spectrum analyzer (ANDO AQ-6315A), and an optical attenuator (Att) was used to control the coupling strength. Before exploring the dynamics of the two mutually coupled semiconductor lasers, we ensured that the laser wavelengths and powers were as well matched as possible by adjusting the laser temperatures and bias currents to avoid frequency detuning (Figure 3.3(a)). The threshold currents of the solitary lasers are $I_{th1} = 12.0$ mA and $I_{th2} = 12.6$ mA, and the explored bias currents were $I_1 = 12.4$ mA ($1.03I_{th1}$) and $I_2 = 13.3$ mA ($1.05I_{th2}$).

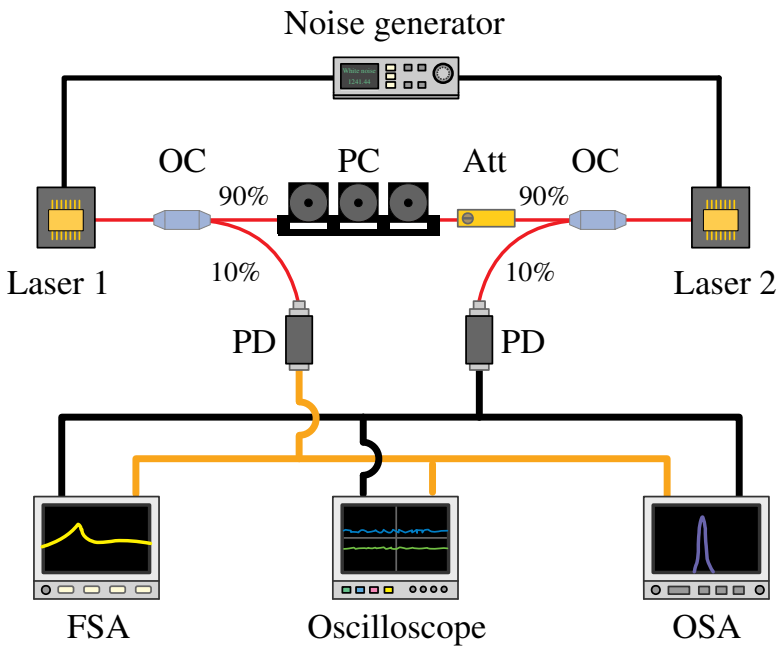

Figure 3.2: Experimental setup. PC: polarization controller, OC: output coupler, Att: optical attenuator, PD: photodetector, FSA: frequency spectrum analyzer, and OSA: optical spectrum analyzer. The red wire represents the single-mode optical fiber, and the black and yellow ones represent the electrical connections.

The same Gaussian noise was applied to the pump currents of both lasers from a noise generator (HP 33120A, 10-MHz bandwidth). Since the internal spontaneous emission noise intrinsic to any semiconductor laser cannot by itself be rectified, the control effort can only be applied on the external noise. Figure 3.3(b) shows frequency spectra of the applied Gaussian noise for different noise amplitude values, and the frequency spectrum of the output intensity in the low-frequency fluctuations regime.

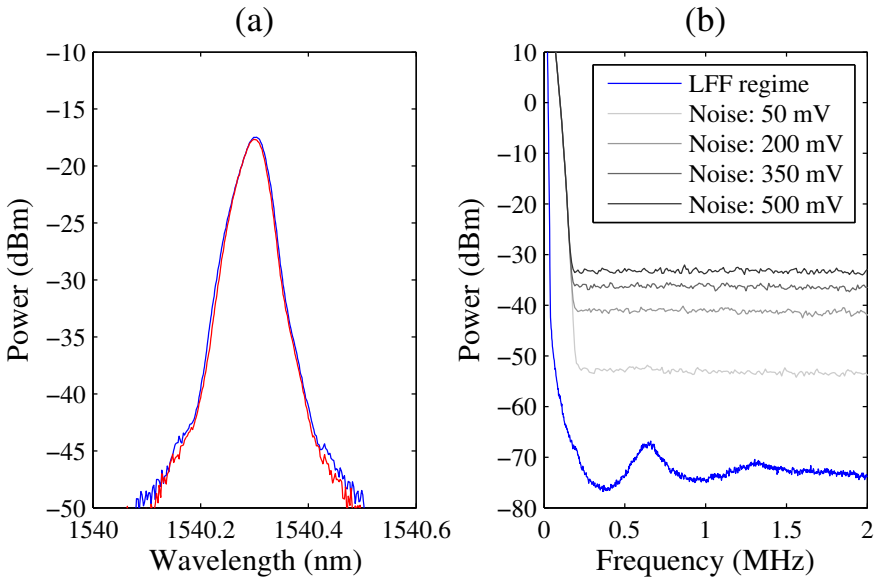

Figure 3.3: (a) Optical spectrum of the two solitary lasers centered at $\lambda = 1540.3$ nm. (b) Power spectrum of noise (upper gray traces) and laser intensity in the low-frequency fluctuations regime (lower blue trace) averaged over 100 realizations. The average frequency of the low-frequency fluctuations is about 0.65 MHz.

3.4 Time series analysis

Depending on the laser parameters and attenuation, the semiconductor lasers exhibited various dynamical regimes: continuous wave emission, chaos, or low-frequency fluctuations. For a relatively strong coupling, the lasers operated in the low-frequency fluctuations regime and when external noise was applied, the windows of a steady-state emission appeared in the time series. A probable mechanism for such noise-induced intermittency is the influence of noise on the stability of the coexisting fixed point. The intermittent switches were detected when the external noise intensity N exceeded a threshold value $N_{th} = 109$ mV.

The intermittency observed was characterized with a time series statistical ana-

lysis. For every noise value, we recorded 100 time series, each of 50 ms length (Figure 3.4). At this resolution, the shortest laminar length we were able to measure was about 0.12 ms (equivalent to around 70 intensity drops of the low-frequency fluctuations considering that their average frequency was 0.65 MHz), while the longest laminar length was almost 50 ms.

With these experimental measurements, the mean duration of the low-frequency fluctuations windows and the probability distribution of the laminar length in the whole 5-s time interval were calculated.

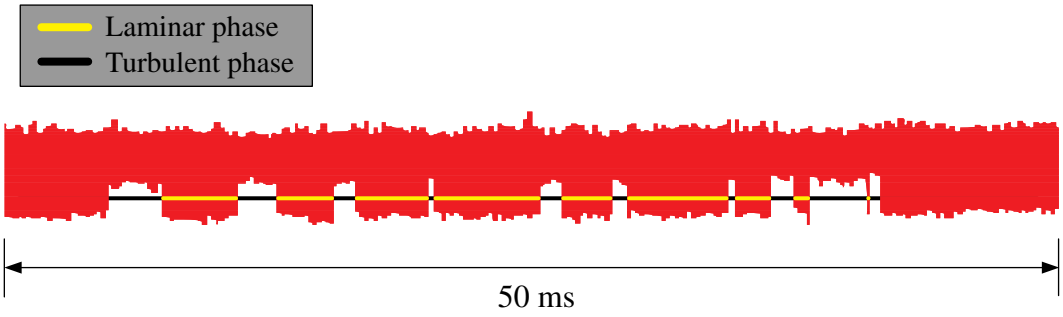

Figure 3.4: Time series of laser intensity showing on–off intermittency for a noise amplitude of 240-mV. The clear windows represent the time intervals in which there were no low-frequency fluctuations. At this resolution, the shortest laminar length we were able to measure was about 0.12 ms, while the longest laminar length was almost 50 ms.

Since the number of switching events depends on the noise intensity, near the onset of intermittency the number of power drops is very small. For that reason, at low noise values, time series were recorded up to 5 s. However, with increasing noise intensity the number of switching events grows exponentially, what significantly improves the statistics.

Figure 3.5 shows the mean laminar length versus the external noise intensity used as a control parameter. In a linear scale, the relationship is well represented by an exponential decay, as shown in Figure 3.5(a). In a log–log scale and close to the onset of intermittency, the mean laminar phase seems to obey a power law with critical exponent close to -1. (Figure 3.5(b)). Since the scaling exponent of -1 has been proven to be a typical characteristic of on–off intermittency, this first analysis suggested that this could be the type of intermittency our system undergoes.

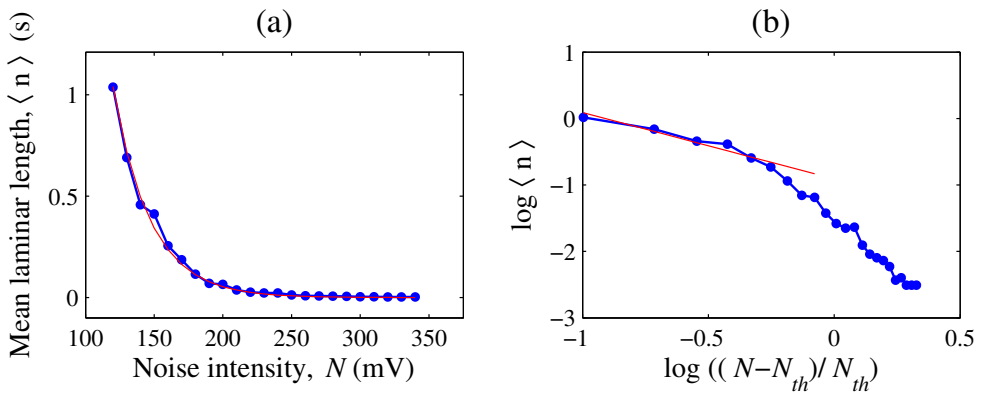

Figure 3.5: Mean laminar length versus noise intensity in (a) linear and (b) log–log scales. The red traces represent (a) an exponential fit, and (b) a line with a slope of -1. $N_{th} = 109$ mV.

Another important intermittency feature is the laminar phase distribution. Figure 3.6 shows the probability distribution of the laminar phases in linear (Figure 3.6(a)) and log–log (Figure 3.6(b)) scales, calculated at a noise intensity of 340-mV. At higher noise values, there were more switching events in the time series, what enabled a better precision of the statistical analysis. In this figure, it is more evident that the probability distribution obeys a power law with a critical exponent close to -3/2, what is a very important feature of on–off intermittency.

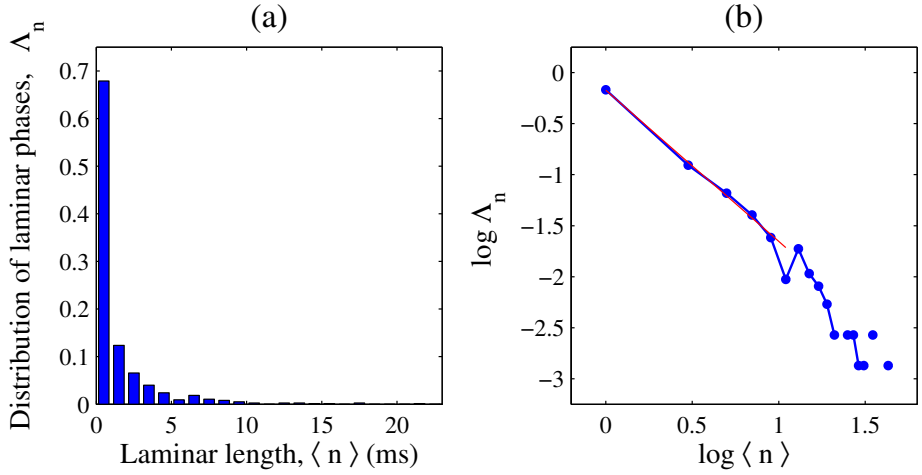

Figure 3.6: Probability distribution of laminar phases versus laminar length at $N = 340$ mV in (a) linear and (b) log–log scales. The red trace represents a line with a slope of -1.5. $N_{th} = 109$ mV.

3.5 Power spectrum analysis

Now, we will show that the intermittency observed can be also characterized by a power-law scaling for the signal-to-noise ratio obtained from the frequency spectrum analysis. Figure 3.7 shows the typical power spectrum (averaged over 100 realizations) of the laser intensity in the intermittency regime. The spectral component S_{LFF} with the central frequency of approximately 0.65 MHz reflects the contribution of the low-frequency fluctuations, while the noise contributes mainly to the background spectral component S_N [88]. As the noise intensity is increased, S_{LFF} decreases while S_N increases, thus leading to the complete disappearance of the low-frequency fluctuations spectral component.

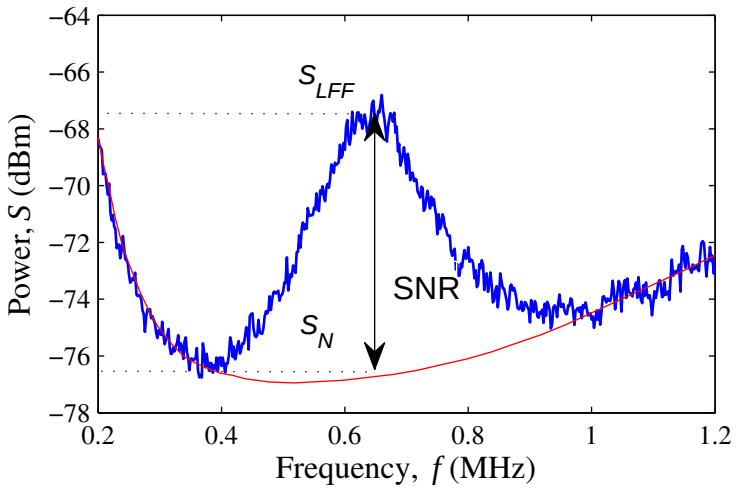

Figure 3.7: Laser power spectrum in the intermittency regime (upper blue trace) and noise background (red lower trace) averaged over 100 realizations. The signal-to-noise ratio (SNR) is measured as an excess of the low-frequency fluctuations spectral component S_{LFF} over the background noise S_N at the central frequency of low-frequency fluctuations (about 0.65 MHz).

To obtain the scaling relation from the power spectrum, we performed a cubic spline interpolation to obtain a soft trace around the spectral peak and on its base. Then, we measured the signal-to-noise ratio SNR $= S_{LFF} - S_N$ (dBm) at the central frequency (0.65 MHz) of the low-frequency fluctuations regime as a function of the noise intensity.

Figure 3.8 shows this dependence in semilog (Figure 3.8(a)) and log–log scales (Figure 3.8(b)). Close to the intermittency onset, a linear fit is a good approximations up to a 340-mV noise. For stronger noise, the SNR approaches zero because the low-frequency fluctuations windows almost disappear in the time series, while

a noisy steady state tendency becomes apparent. The red trace in Figure 3.8(b) shows that near the onset of intermittency, the signal-to-noise ratio versus the normalized noise intensity obeys a power law with a critical exponent of -1. This result is more evident and is in agreement with the scaling relation obtained from the time series analysis (compare with Figure. 3.5). Such agreement reflects the fact that the averaged S_{LFF} is associated with the mean duration of the laminar phase. The frequency spectra analysis resulted simpler and faster than the statistical treatment of the time series.

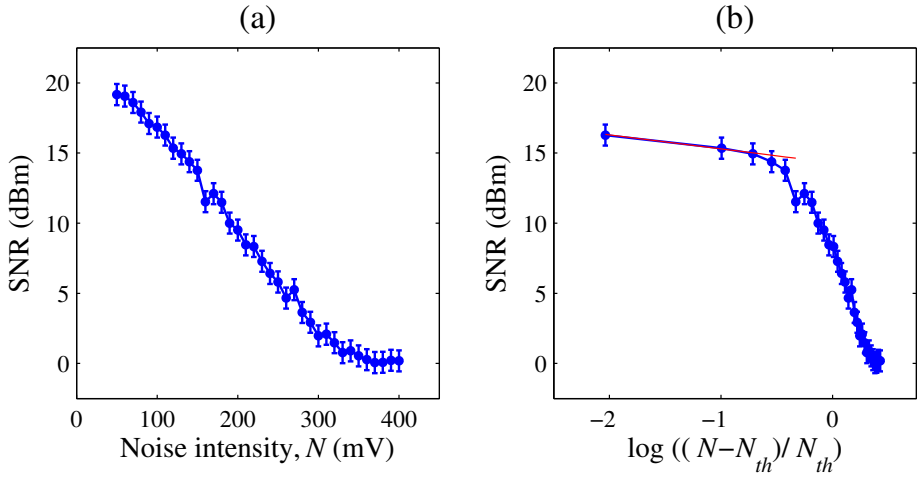

Figure 3.8: Signal-to-noise ratio versus noise intensity in (a) semilog and (b) log–log scales. The error bars represent the maximum error in the determination of the frequency spectral peak. The red trace is a line with a slope of -1.

3.6 Conclusion

Intermittent switches between a steady-state emission and a regime of low-frequency fluctuations have been observed in experiments with two mutually coupled semiconductor lasers when common Gaussian noise was applied to the laser pump currents. The time series analysis revealed power laws for the intermittency observed. Near the onset of intermittency, the mean laminar length was found to obey a -1 power law with respect to the normalized noise intensity, while the probability distribution of the laminar phases over the laminar length displayed a -3/2 power law. These two scaling relations are consistent with the key signature of on–off intermittency. Besides, the time-dependent modulation of a bifurcation parameter through a bifurcation point required by on-off intermittency was provided by the random modulation of the pump current of both lasers. Furthermore, the analysis of the average power spectra revealed a -1 scaling exponent for the signal-to-noise ratio versus the noise intensity exhibiting a good agreement with the scaling law found from

the time series. Such agreement reflects the fact that the averaged low-frequency fluctuations spectral component S_{LFF} is associated with the mean duration of the laminar phase.

Chapter 4

Dual-cavity laser dynamics

4.1 Abstract

We experimentally studied the dynamics of a dual-cavity Nd:YAG laser with second harmonic generation in one of the cavities and loss modulation in the second one. Depending on the frequency of harmonic modulation of the infrared light, we observed the coexistence of different correlated and uncorrelated regimes of the infrared and green outputs from the two laser cavities. We present experimental evidence of the existence of the dynamical regime of oscillation death in the green and infrared output intensities of the laser, coexistent with oscillatory states for certain values of the loss modulation frequency that was used as a control parameter.

4.2 Introduction

Fast development of laser technology faces technological problems which require special attention. One famous example is the so-called "green problem" [19] present in a Nd:YAG laser with a nonlinear crystal in the cavity. The intracavity frequency-doubled crystal converts the infrared (IR) light at the 1.06-μm wavelength into green light at a wavelength of 532 nm. The nonlinear coupling between modes in the second harmonic generation (SHG) crystal gives rise to irregular fluctuations of the laser power. This irregular behavior was largely investigated and attributed to the destabilization of relaxation oscillations, always existent in this kind of lasers due to nonlinear coupling of longitudinal modes. In spite of numerous attempts to stabilize steady states by various feedback control methods [89], the success was insignificant.

Another reason of instabilities in this laser is the coexistence of multiple attractors, where the irregularity in the laser intensity may lie in aleatory switches between the coexisting states induced by noise or any external interference [31]. This work was motivated by a search of possibilities to control this kind of irregular laser be-

havior. One possible approach would be attractor annihilation by external harmonic modulation [90, 91].

Synchronization of coupled chaotic systems [23, 92–94], including lasers [95–97] has been widely investigated over the past few decades. The Nd:YAG laser with intracavity potassium titanium oxide phosphate ($KTiOPO_4$), or KTP crystal is a system of special interest because it is a highly efficient source of visible coherent light. Moreover, chaotic Nd:YAG lasers have proved to be ideal candidates for multichannel communication [98]. Chaotic synchronization of multimode Nd:YAG lasers could be used in digital communication of two-dimensional messages. Since in a multimode laser, chaotic synchronization between corresponding cavity modes differs from that between different cavity modes, each pair of corresponding cavity modes could be used as a channel in an optical communication system.

One very interesting synchronous state is referred to as *oscillation death*, and it deals with the absence of oscillations in a coupled system, whereas each subsystem oscillates when isolated. This type of synchronization was theoretically investigated by several researchers [99–104] and experimentally demonstrated in chemical [105], optical [106], and electronic systems [107]. The majority of papers are devoted to the oscillation death in autonomous (self-oscillatory) systems, with a small exclusion [30, 108] which reports on the observation of similar phenomenon in nonautonomous (forced) systems. While in the former case, the oscillation death appears due to a time delay in coupling, in the latter case the dead states arise in a saddle-node bifurcation which gives rise to a stable fixed point coexistent with a limit cycle or chaos [30]. Thus, the oscillation death in nonautonomous systems is related to the emergence of multistability. This has been numerically demonstrated in the coupled Duffing oscillators [30] and in a dual-cavity CO_2 laser with modulated losses in one of the cavities [108].

In this work, we present experimental evidence of oscillation death in a periodically forced system, and show its relation to the multistabilty emergence in a dual-cavity Nd:YAG laser with a second harmonic generation crystal in one cavity and loss modulation in another cavity. Our interest is centered in cooperative dynamics and synchronization of the infrared and green outputs from the two laser cavities.

4.3 Experimental setup

Figure 4.1 shows the optical scheme of our experimental setup. The experiments were carried out with a diode-pumped Nd:YAG laser with a KTP crystal for second harmonic generation, which was placed inside one of the laser cavities. Another

cavity was formed by a beam splitter (BS) and an additional mirror so that the active medium (Nd:YAG) was present in both cavities. An electro-optical modulator (EOM) and the second harmonic generation crystal were placed in different cavities; the one with the electro-optical modulator was the active cavity and the cavity with the second harmonic generation crystal was the passive one. A harmonic signal from a signal generator (SG) was applied to the electro-optical modulator in order to modulate losses in the active cavity. An infrared filter (IRF) placed in front of the electro-optical modulator allowed modulating the infrared light only. Another infrared filter put in front of a photodetector (PD) served for cutting the green light. A green filter (GF) placed in front of another photodetector blocked the infrared light allowing the detection of the green light only from the passive cavity. Thus, by modulating only the infrared light we recorded both the infrared and green laser radiation components.

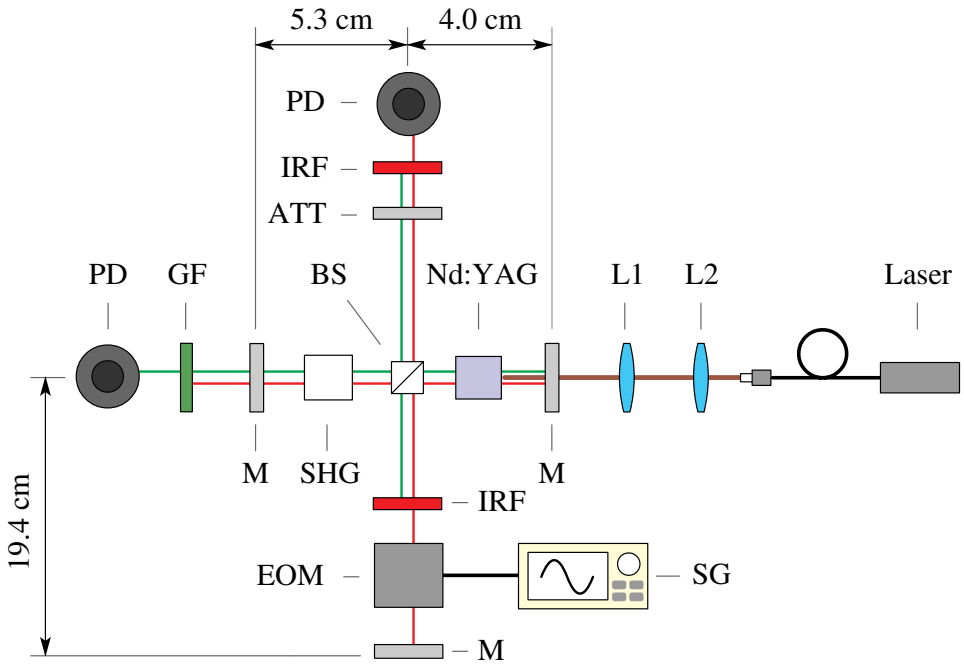

Figure 4.1: Optical scheme of a diode-pumped dual-cavity Nd:YAG laser with a second-harmonic generation crystal (SHG) in the passive cavity and an electro-optical modulator (EOM) in the active cavity. PD: photodetector, M: cavity mirrors, BS:polarizing beam splitter, IRF: infrared filter, GF: green filter, ATT: variable attenuator, L1: focusing lens, L2: collimating lens, SG: signal generator, and Laser: diode pump laser. The dark red line represents the diode pump laser emission, the red one represents the infrared light from the Nd:YAG laser, and the green line the frequency-doubled light.

For the pumping we used a diode laser (BWT K81S09F-8.00W, 808 nm) with current (BK Precision 1696) and temperature (Newport 350B) controllers. The laser

outputs were recorded by two photodetectors (Thorlabs PDA 36A, 350–1100nm wavelength range, 17-MHz bandwidth) and visualized with an oscilloscope (Tektronix DPO 7104, 3.5-GHz bandwidth). The harmonic waveform was obtained with a function generator (Tektronix AFG 3021B). For loss modulation we used an electro-optical amplitude modulator (Thorlabs EO-AM-NR-C2, 900-1250nm) with a high voltage amplifier (Thorlabs EO-HVA). The threshold currents for the diode pump and Nd:YAG lasers were respectively $I_{th}^{p} = 1.6$ A and $I_{th}^{Nd} = 2.6$ A.

The diode laser used for the pumping was operated at a current of $I = 4.016$ A ($1.5I_{th}$) and a temperature of 23.0 °C. With these parameters and after a careful alignment of the optical components in the two cavities, the infrared optical power measured within the passive cavity was $I_{IR} = 35.6$ mW, and the green optical power was $I_g = 1.8$ mW, that is, the second-harmonic conversion efficiency was just above 5%.

4.4 Synchronization

The modulation of the infrared light resulted in modulation of the green light because of nonlinear coupling through the active medium and the second-harmonic generation crystal. Figure 4.2(a) shows the bifurcation diagrams of the laser peak intensities of the IR and green outputs. The diagrams were constructed by plotting peak intensities of the last 100 local maxima of the time series for every modulation frequency f taken with a 500-Hz step at fixed diode pump current equal to 4 A. The duration of the recorded time series ranged from 100 ms for $f = 5$ kHz to 1 ms for $f = 500$ kHz.

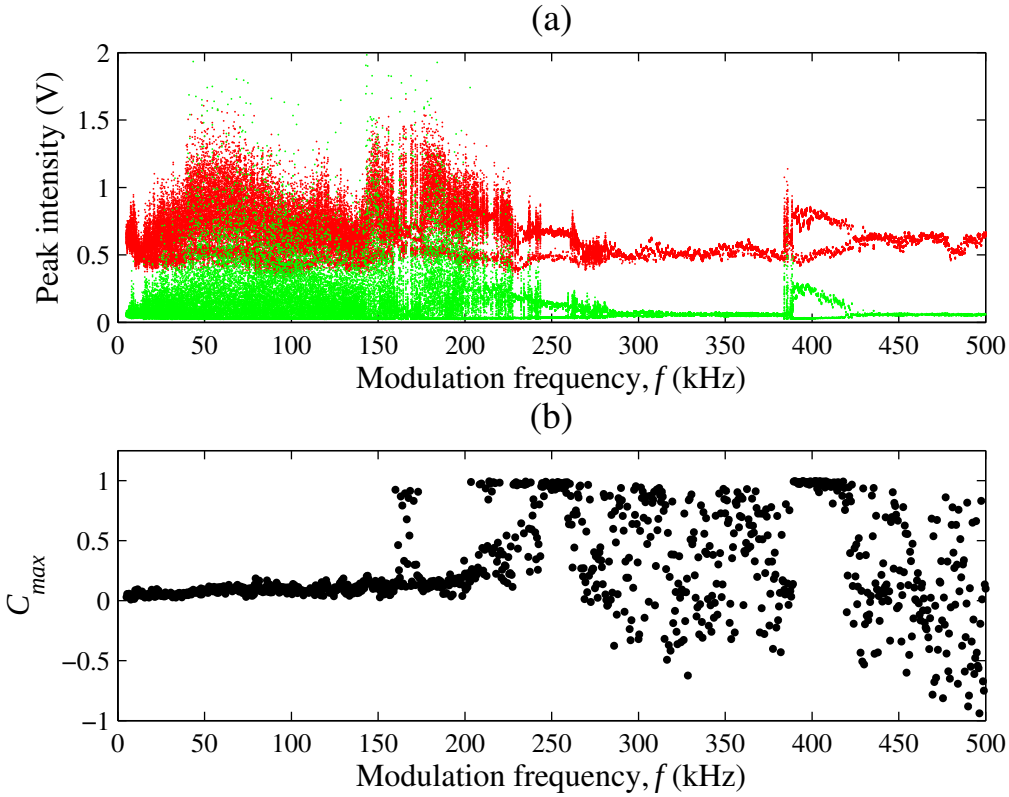

Figure 4.2: Bifurcation diagrams of (a) laser peak intensities of infrared (upper trace) and green (lower trace) outputs, and (b) maximum cross-correlation (C_{max}) between them versus modulation frequency.

Synchronization of the IR and green laser components can be quantitatively measured with the cross-correlation function of the two temporal waveforms, defined as [10, 22, 109]

$$C = \frac{\big\langle \big(I_{IR,\,i} - \langle I_{IR}\rangle\big)\big(I_{g,\,i} - \langle I_g\rangle\big)\big\rangle}{\sigma_{IR}\,\sigma_g}\,, \tag{4.1}$$

where $I_{IR,\,i}$ and $I_{g,\,i}$ are the ith sampled point of the temporal waveform of the IR and green laser intensities. $\langle I_{IR}\rangle$ and $\langle I_g\rangle$ are the mean values of $I_{IR,\,i}$ and $I_{g,\,i}$, defined as

$$\langle I_{IR}\rangle = \frac{1}{N}\sum_{i=1}^{N} I_{IR,\,i}\,, \tag{4.2}$$

$$\langle I_g \rangle = \frac{1}{N} \sum_{i=1}^{N} I_{g,\,i} \ , \tag{4.3}$$

where N is the total number of points sampled from the temporal waveforms. σ_{IR} and σ_g are the standard deviations of $I_{IR,\,i}$ and $I_{g,\,i}$, defined as

$$\sigma_{IR} = \sqrt{\frac{1}{N} \sum_{i=1}^{N} (I_{IR,\,i} - \langle I_{IR} \rangle)^2} \ , \tag{4.4}$$

$$\sigma_g = \sqrt{\frac{1}{N} \sum_{i=1}^{N} (I_{g,\,i} - \langle I_g \rangle)^2} \ . \tag{4.5}$$

The value of C in Equation (4.1) ranges from -1 to 1. The best inphase synchronization of chaos is obtained at the cross-correlation value of $C = 1$. The best antiphase synchronization of chaos is obtained at C = -1. No synchronization is observed at $C = 0$.Figure 4.2(b) shows the maximum cross-correlation between the IR and green lights as a function of the modulation frequency. In the bifurcation diagrams in Figure 4.2, one can distinguish several critical points, where the laser changed its behavior. In particular, the bifurcations appeared at $f \approx 160$ kHz, $f \approx 240$ kHz, $f \approx 260$ kHz, $f \approx 390$ kHz, and $f \approx 420$ kHz. The time series analysis allowed us to characterize these bifurcations and associate some of them with saddle-node and Hopf bifurcations.

In the low-frequency range $f < 160$ kHz, the laser oscillated in a chaotic regime, where the IR and green components were uncorrelated ($C_{max} \approx 0$), i.e. no synchronization was observed (Figures 4.3(a,b)). The emergence of multistability at $f \approx 160$ kHz allowed us to associate this point with a saddle-node bifurcation. For $f > 160$ kHz different cross-correlations corresponded to different coexisting states. When the laser was in the periodic regime (Figures 4.3(c,d)), the IR and green components were strongly correlated ($C_{max} \approx 1$) and the oscillation frequencies were locked to a certain ratio with the external modulation frequency. The phases were also locked at a certain phase difference between the outputs, as seen from Figures 4.3(c–f). Instead, when one of the outputs was in a chaotic regime and another one in a periodic regime (Figures 4.4(b,d)), the correlation was very low. Therefore, the cross-correlation in the multistable region was uncertain, i.e. C_{max} could take different values between 0 and 1 depending on the attractors released.

The cross-correlation was also uncertain in the range 270 kHz $< f <$ 390 kHz

when the laser was in the regime of oscillation death, i.e. when both outputs displayed a noisy steady state emission (Figure 4.5(f)). The bifurcations at $f \approx 390$ kHz and $f \approx 420$ kHz we referred, respectively, to as Hopf and inverse Hopf bifurcations because at the former point a steady state converted to a periodic orbit and at the latter point a periodic orbit converted to a steady state.

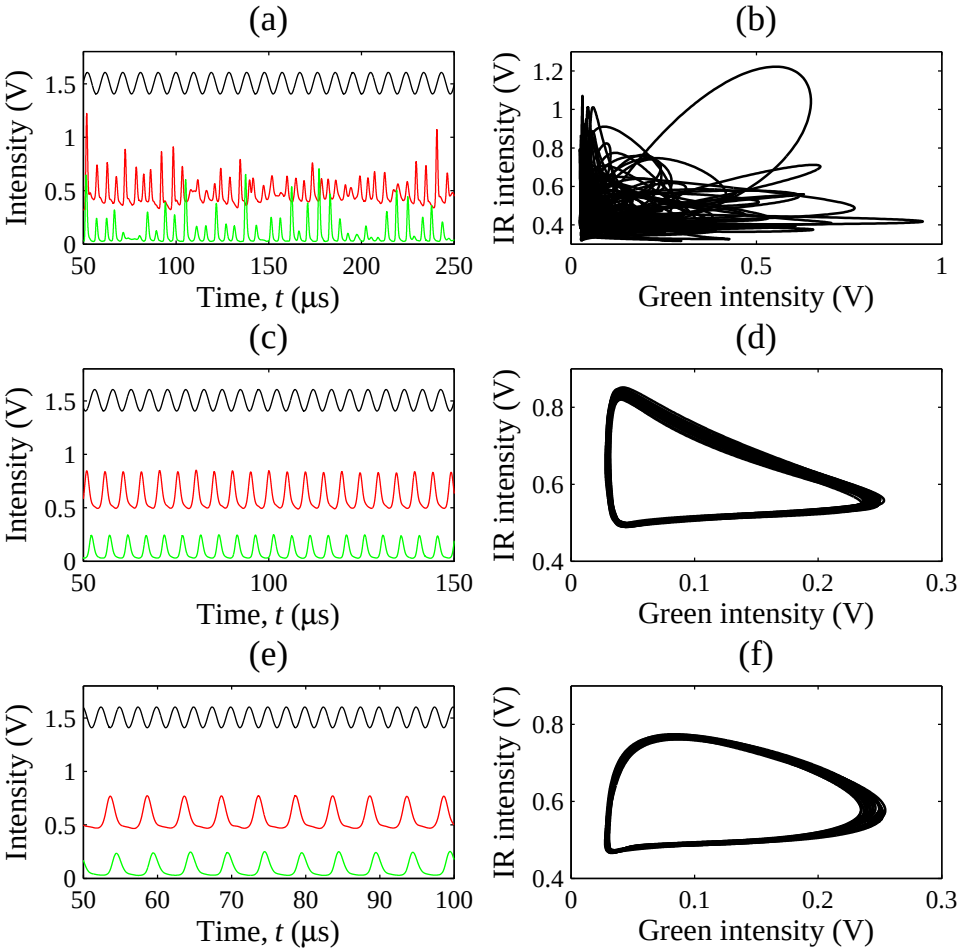

Figure 4.3: Time series (left) and phase-space plots (right) of IR (middle traces) and green (lower traces) laser outputs demonstrating dynamical regimes with different rotation numbers. (a,b) 2:1 chaotic regime at $f = 100$ kHz, (c,d) 1:1 periodic regime at $f = 203.5$ kHz, and (e,f) 1:2 periodic regime at $f = 400$ kHz. The upper (black) traces represent the modulating signal. They are shown rescaled and shifted vertically only for visualizing purposes.

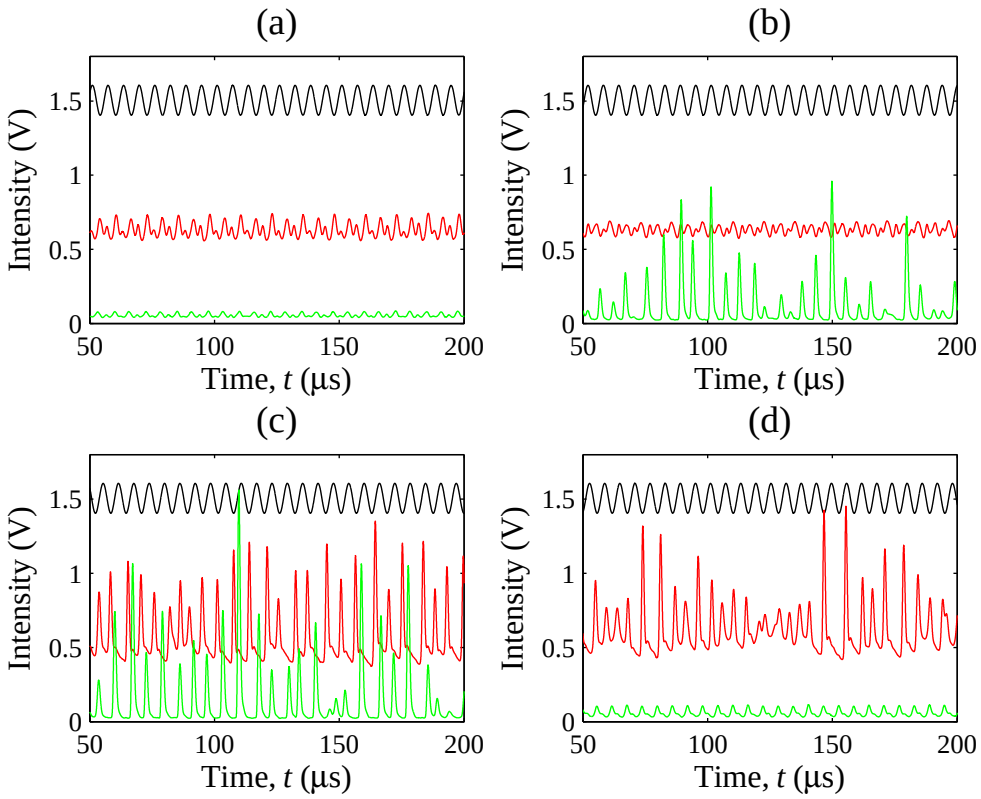

Figure 4.4: Coexistence of attractors near $f \approx 163$ kHz. (a) The infrared (middle trace) and green (lower trace) components are in periodic regimes ($f = 160$ kHz), (b) infrared is in a periodic and green is in a chaotic state (162 kHz), (c) both infrared and green outputs are chaotic (162.5 kHz), and (d) infrared is in chaos and green is in a period 1 (165 kHz). The upper (black) traces represent the modulating signal. They are shown rescaled and shifted vertically only for visualizing purposes.

4.5 Coexisting attractors and oscillation death

In Figure 4.4 we show the time series corresponding to four different coexisting regimes detected in the vicinity of 163 kHz. A small variation of f resulted in switches between coexisting attractors due to changes in the initial conditions. Multistability was observed for modulation frequencies near 90 kHz (Figures 4.5(a,b)), 160 kHz $< f <$ 260 kHz (Figures 4.5(c,d)), and 380 kHz $< f <$ 420 kHz (Figures 4.5(e,f)). In the last region we found the coexistence of oscillatory and steady state regimes. We attribute the latter regime to oscillation death shown in Figure 4.5(f). The stable steady state always coexisted with a limit cycle as predicted in Ref. [30].

The origin of the oscillation death may lie in a sufficiently large difference between

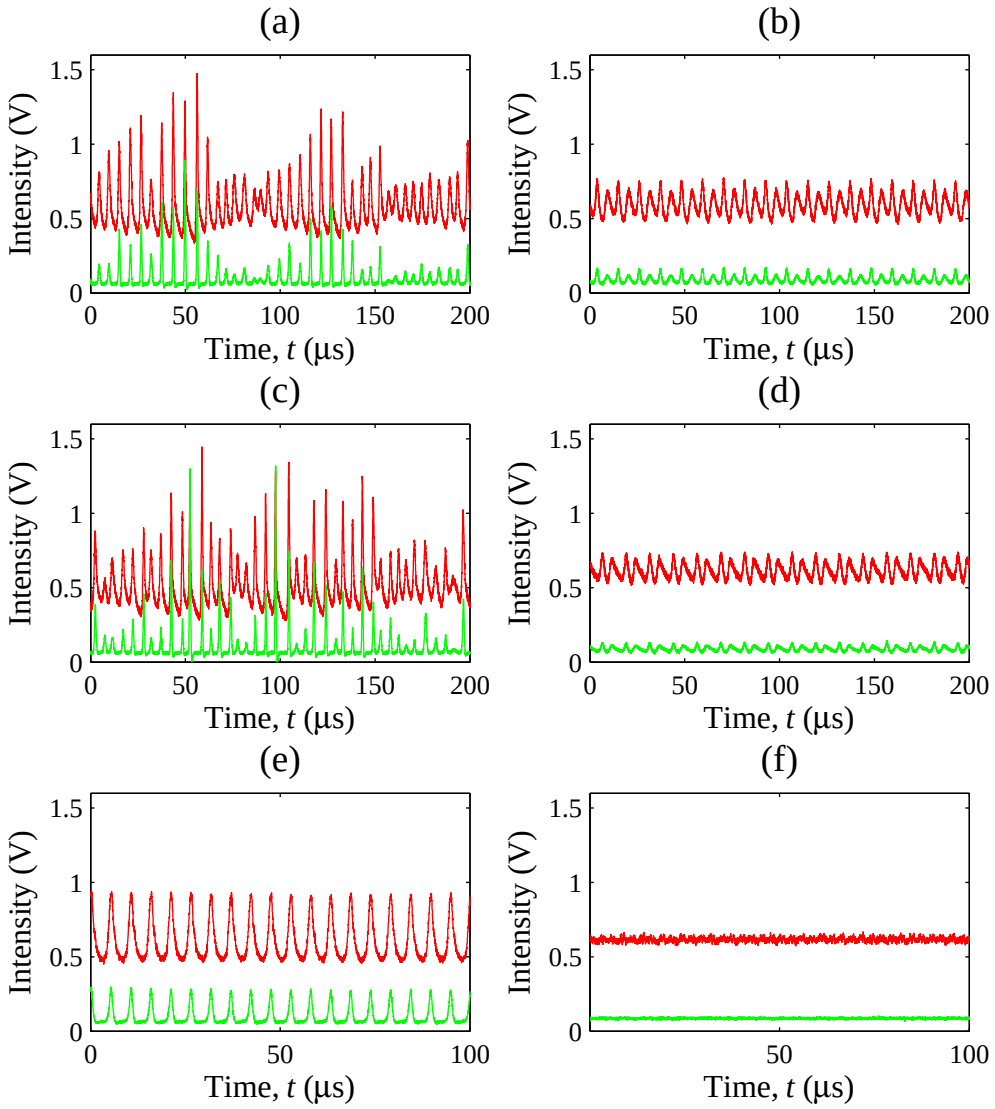

Figure 4.5: Coexistence of (a,c) chaotic and (e) periodic regimes with (b,d) periodic and (f) steady state regimes at modulation frequencies (a,b) $f = 90$ kHz, (c,d) 200 kHz, and (e,f) 380 kHz.

natural laser frequencies for the IR and green components because of the difference in their gains and cavity losses, so that the coupling in the active medium creates a saddle-node pair of fixed points on the limit cycle [110].

4.6 Conclusions

We experimentally studied dynamics of a dual-cavity Nd:YAG laser with second harmonic generation under harmonic loss modulation of the infrared laser component. Depending on the modulation frequency, chaotic, periodic, and steady state regimes were observed. Synchronization of the IR and green laser lights was investigated using a cross-correlation function. In certain regions of the modulation frequency, multistability was detected; chaotic orbits coexisted with periodic orbits. When the laser operated in a chaotic regime, the oscillations of the IR and green components were uncorrelated, whereas in a periodic regime they were strongly correlated and their frequencies and phases were locked. We also observed the coexistence of oscillatory and steady state regimes. The latter is attributed to oscillation death, i.e. the absence of oscillations in both laser components, that may arise from the difference between natural laser frequencies for the IR and green lights, due to their cooperative dynamics. This experimental evidence of the oscillation death in the periodically forced system confirmed previous theoretical predictions [30, 108].

Chapter 5

General conclusions

In this thesis we have studied experimentally stochastic effects such as coherence enhancement, noise-induced intermittency, and amplitude death in multistable semiconductor and solid-state lasers.

We presented evidence of noise-induced intermittency in an optically injected semiconductor laser at the boundary of the frequency-locking regime, and the existence of an optimal master laser pump current for the coherence enhancement. We also found that the inter-spike interval fluctuations in the intermittency regime obeyed a non-Gaussian stable distribution. In the intermittent regime, the characteristic exponent, α, was almost constant, while the scale parameter, γ, had a minimum at the current value corresponding to maximum coherence. We consider that this laser configuration could be useful in an optical communication system that could exploit the existence of two states in the optical output of the slave laser. Additionally, these results could contribute to the improvement of the quality of the communications in this type of systems.

Also, intermittent switches between a steady-state and a regime of low-frequency fluctuations were observed in experiments with two mutually coupled semiconductor lasers subject to common Gaussian noise applied to their laser pump currents. The two scaling relations derived from the time series are consistent with the key signature corresponding to on–off intermittency. Furthermore, the analysis of the average power spectra revealed a good agreement with the scaling law found from the time series analysis. We consider that this research could help in the understanding of the positive effects of noise in the dynamics of laser systems.

Additionally, we studied the rich dynamics of a dual-cavity Nd:YAG laser with second harmonic generation under harmonic loss modulation of the infrared laser component, and multistability was detected for certain regions of the modulation frequency. When the laser operated in a chaotic regime, the oscillations of the infrared and green components were uncorrelated, whereas in a periodic regime they

were strongly correlated and their frequencies and phases were locked. The observed coexistence of oscillatory and steady state regimes, which we attribute to oscillation death, may arise due to cooperative dynamics from the difference between natural laser frequencies for the infrared and green lights. Besides the contribution of this work from the nonlinear dynamics point of view, we consider that the obtained results may be relevant in optical communication systems as Nd:YAG lasers have proved to be candidates for multichannel communications and because chaotic synchronization of this kind of multimode lasers could be used in digital communication with two-dimensional messages since each pair of corresponding cavity modes could be used as a channel in optical communications due to the fact that chaotic synchronization between corresponding cavity modes differs from the synchronization between different cavity modes.

As a future work in the short term, we want to explore the following research lines:

1. Use other slave laser pump currents to investigate the presence and characteristics of coherence enhancement of intermittency and to make a map with both laser pump currents as control parameters.

2. Make a numerical study of the coherence enhancement to corroborate the experimental results that we have. This study would be based on the Lang-Kobayashi laser equations that describe a semiconductor laser with external optical feedback.

3. Study rogue waves in the same experimental array. This is motivated on partial experimental results that we did that suggest that the phenomenon might be present in this laser configuration.

4. Use the Lang-Kobayashi model to make a numerical study of the on-off intermittency that was found in the study of two mutually coupled semiconductor lasers.

5. Investigate the emergence of multistability and synchronization in the dual-cavity Nd:YAG laser with second-harmonic generation in one of the cavities that was described in chapter 4, but using the optical pumping and the amplitude of the loss modulation as control parameters.

Appendix A

Publications

1. A. Campos-Mejía, A. N. Pisarchik, and D. A. Arroyo-Almanza, *Noise-induced on–off intermittency in mutually coupled semiconductor lasers*, Chaos, Solitons and Fractals, 54, 2013.

2. A. Campos-Mejía, A. N. Pisarchik, V. Pinto-Robledo, R. Sevilla-Escoboza, R. Jaimes-Reátegui, G. Huerta-Cuellar, V. P. Vera-Avila, *Synchronization of infrared and green components in a loss-modulated dual-cavity Nd:YAG laser with second harmonic generation*, European Physics Journal (Special Topics), 223(13), 2014.

3. A. Campos-Mejía, A. N. Pisarchik, R. Sevilla-Escoboza, G. Huerta-Cuellar, and V.P. Vera-Ávila, *Coherence enhanced intermittency in an optically injected semiconductor laser*, Optics Express, 23(8), 2015.

Bibliography

[1] S. H. Strogatz, *Nonlinear Dynamics and Chaos*. Westview Press, 2001.

[2] E. Ott, *Chaos in Dynamical Systems*. Cambridge University Press, 1993.

[3] R. M. May, "Simple mathematical models with very complicated dynamics," *Nature*, vol. 261, pp. 459–, 1976.

[4] E. N. Lorenz, "Deterministic nonperiodic flow," *J. Atmos. Sci.*, vol. 20, p. 130–141, 1963.

[5] S. Johansson and V. Letokhov, "Astrophysical lasers and nonlinear optical effects in space," *New Astronomy Reviews*, vol. 51, pp. 443–523, 2007.

[6] A. Einstein, "Zur quantentheorie der strahlung," *Physikalische Zeitschrift*, vol. 18, pp. 121–128, 1917.

[7] J. P. Gordon, H. J. Zeiger, and C. H. Townes, "The maser—new type of microwave amplifier, frequency standard, and spectrometer," *Physical Review*, vol. 99, no. 4, pp. 1264–, 1955.

[8] T. H. Maiman, R. H. Hoskins, I. J. D'Haenens, C. K. Asawa, and V. Evtuhov, "Stimulated optical emission in fluorescent solids. ii. spectroscopy and stimulated emission in ruby," *Physical Review*, vol. 123, no. 4, pp. 1151–, 1961.

[9] V. Aboites, *El láser*. FCE, 1991.

[10] A. Uchida, *Optical Communications with Chaotic Lasers*. Wiley-VCH, 2012.

[11] V. Aboites, *Láseres, una Introducción*. CIO, 1991.

[12] O. Svelto, *Principles of Lasers*. Springer, 2009.

[13] R. Hall, G. Fenner, J. Kingsley, T. J. Soltys, and R. O. Carlson, "Coherent light emission from gaas junctions," *Phys. Rev. Lett.*, vol. 9, no. 9, p. 565–577, 1962.

[14] G. H. M. van Tartwijk and D. Lenstra, "Semiconductor lasers with optical injection and feedback," *Quantum Semiclass.*, vol. 7, pp. 87–143, 1995.

[15] J. E. Geusic, H. M. Marcos, and L. G. van Uitert, "Laser oscillations in nd-doped yttrium aluminum, yttrium gallium and gadolinium garnets," *App. Phys. Lett.*, vol. 4, no. 10, pages =182-184, year =1964.

[16] A. Yariv, *Optical Electronics*. Saunders College Publishing, 1991.

[17] D. A. Arroyo-Almanza, A. N. Pisarchik, and F. R. Ruiz-Oliveras, "Route to chaos in a ring of three unidirectionally-coupled semiconductor lasers," *IEEE Phot. Tech. Lett.*, vol. 24, no. 7, pp. 605–607, 2012.

[18] J. Ohtsubo, *Semiconductor Lasers: Stability, Instability and Chaos*. Springer-Verlag, 2008.

[19] T. Baer, "Large-amplitude fluctuations due to longitudinal mode coupling in diode-pumped intracavity-doubled nd:yag lasers," *J. Opt. Soc. Am. B*, vol. 3, no. 9, pp. 1175–1180, 1986.

[20] H. Haken, "Analogy between higher instabilities in fluids and lasers," *Phys. Lett. A*, vol. 53, no. 1, p. 77–78, 1975.

[21] F. T. Arecchi, G. L. Lippi, J. G. P. Puccioni, and Tredicce, "Deterministic chaos in laser with injected signal," *Opt. Comm.*, vol. 51, no. 5, p. 308–314, 1984.

[22] D. Arroyo-Almanza, A. Pisarchik, I. Fischer, C. Mirasso, and M. Soriano, "Spectral properties and synchronization scenarios of two mutually delay-coupled semiconductor lasers," *Opt. Comm.*, vol. 301, pp. 67–73, 2013.

[23] A. Pikovsky, M. Rosenblum, and J. Kurths, *Synchronization: A Universal Concept in Nonlinear Science*. Cambridge University Press, 2001.

[24] M. Bennett, M. Schatz, H. Rockwood, and K. Wiesenfeld, "Huygens's clocks," *Proc. R. Soc. Lond. A*, vol. 458, no. 2019, pp. 563–579, 2002.

[25] L. M. Pecora and T. L. Carroll, "Synchronization in chaotic systems," *Phys. Rev. Lett.*, vol. 64, no. 8, pp. 821–824, 1990.

[26] N. F. Rulkov, M. M. Sushchik, L. S. Tsimring, and H. D. I. Abarbanel, "Generalized synchronization of chaos in directionally coupled chaotic systems," *Phys. Rev. E*, vol. 51, no. 2, pp. 980–994, 1995.

[27] M. G. Rosenblum, A. S. Pikovsky, and J. Kurths, "Phase synchronization of chaotic oscillators," *Phys. Rev. Lett.*, vol. 76, no. 11, pp. 1804–1807, 1996.

[28] M. G. Rosenblum, A. S. Pikovsky, and J. Kurths, "From phase to lag synchronization in coupled chaotic oscillators," *Phys. Rev. Lett.*, vol. 78, no. 22, pp. 4193–4196, 1997.

[29] H. U. Voss, "Anticipating chaotic synchronization," *Phys. Rev. E*, vol. 61, no. 5, pp. 5115–5119, 2000.

[30] A. Pisarchik, "Oscillation death in coupled nonautonomous systems with parametrical modulation," *Phys. Lett. A*, vol. 318, no. 1, pp. 65–70, 2003.

[31] A. Pisarchik and U. Feudel, "Control of multistability," *Phys. Rep.*, vol. 540, no. 4, pp. 167–218, 2014.

[32] F. Arecchi, R. Meucci, G. Puccioni, and J. Tredicce, "Experimental evidence of subharmonic bifurcations, multistability, and turbulence in a q-switched gas laser," *Phys. Rev. Lett.*, vol. 49, pp. 1217–1220, 1982.

[33] A. Pisarchik, Y. Barmenkov, and A. Kir'yanov, "Experimental characterization of bifurcation structure in an erbium-doped fiber laser with pump modulation," *IEEE J. Quantum. Electron.*, vol. 39, pp. 1567–1571, 2003.

[34] J. Saucedo-Solorio, A. Pisarchik, A. Kir'yanov, and V. Aboites, "Generalized multistability in a fiber laser with modulated losses," *J. Opt. Soc. Am. B*, vol. 20, pp. 490–496, 2003.

[35] C. Vidal and A. Pacault, eds., *Non-Equilibrium Dynamics in Chemical Systems*. Springer Series in Synergetics, 1984.

[36] A. R. Bulsara and L. Gammaitoni, "Tunig in to noise," *Phys. Today*, pp. 39–45, 1996.

[37] L. Gammaitoni, P. Hänggi, P. Jung, and F. Marchesoni, "Stochastic resonance," *Rev. Mod. Phys.*, vol. 70, no. 1, pp. 223–287, 1998.

[38] P. S. Landa and P. McClintock, "Vibrational resonance," *J. Phys. A*, vol. 33, pp. L433–L438, 2000.

[39] A. A. Zaikin, L. López, J. P. Baltanás, J. Kurths, and M. A. F. Sanjuán, "Vibrational resonance in a noise-induced structure," *Phys. Rev. E*, vol. 66, pp. 011106–, 2002.

[40] V. N. Chizhevsky, E. Smeu, and G. Giacomelli, "Experimental evidence of "vibrational resonance" in an optical system," *Phys. Rev. Lett.*, vol. 91, no. 22, pp. 220602–, 2003.

[41] A. S. Pikovsky and J. Kurths, "Coherence resonance in a noise-driven excitable system," *Phys. Rev. Lett.*, vol. 78, pp. 775–, 1997.

[42] J. B. Gao, S. K. Hwang, and J. M. Liu, "Effects of intrinsic spontaneous-emission noise on the nonlinear dynamics of an optically injected semiconductor laser," *Phys. Rev. A*, vol. 59, pp. 1582–1585, 1999.

[43] A. Campos-Mejía, A. N. Pisarchik, and D. A. Arroyo-Almanza, "Noise-induced on–off intermittency in mutually coupled semiconductor lasers," *Chaos, Solitons and Fractals*, vol. 54, pp. 96–100, 2013.

[44] S. Wieczorek and D. Lenstra, "Spontaneously excited pulses in an optically driven semiconductor laser," *Phys. Rev. E*, vol. 69, pp. 016218–, 2004.

[45] N. G. V. Kampen, *Stochastic Processes in Physics and Chemistry*. Elsevier, 1981.

[46] P. Hänggi, P. Talkner, and M. Borkovec, "Reaction-rate theory: fifty years after kramers," *Rev. Mod. Phys.*, vol. 62, p. 251–342, 1990.

[47] D. H. Kawaguchi, K. Inoue, T. Matsuoka, and K. Otsuka, "Bistable output characteristics in semiconductor laser injection locking," *IEEE J. Quantum Electron.*, vol. 21, no. 9, pp. 1314–1317, 1985.

[48] S. Osborne, A. Amann, D. Bitauld, and S. O'Brien, "On-off intermittency in an optically injected semiconductor laser," *Phys. Rev. E*, vol. 85, pp. 056204–, 2012.

[49] D. Ziemann, R. Aust, B. Lingnau, E. Schöll, and K. Lüdge, "Optical injection enables coherence resonance in quantum-dot lasers," *Eur. Phys. Lett.*, vol. 103, pp. 14002–, 2013.

[50] H. Gang, T. Ditzinger, C. Z. Ning, and H. Haken, "Stochastic resonance without external periodic force," *Phys. Rev. Lett.*, vol. 71, pp. 807–810, 1993.

[51] J. L. A. Dubbeldam, B. Krauskopf, and D. Lenstra, "Excitability and coherence resonance in lasers with saturable absorber," *Phys. Rev. E*, vol. 60, pp. 6580–6588, 1999.

[52] J. F. M. Avila, H. L. D. de S. Cavalcante, and J. R. R. Leite, "Experimental deterministic coherence resonance," *Phys. Rev. Lett.*, vol. 93, no. 14, pp. 144101–, 2004.

[53] G. Giacomelli, M. Giudici, S. Balle, and J. R. Tredicce, "Experimental evidence of coherence resonance in an optical system," *Phys. Rev. Lett.*, vol. 84, no. 15, p. 3298–3301, 2000.

[54] O. V. Ushakov, H. J. Wünsche, F. Henneberger, I. A. Khovanov, L. Schimansky-Geier, and M. A. Zaks, "Coherence resonance near a hopf bifurcation," *Phys. Rev. Lett.*, vol. 95, pp. 123903–, 2005.

[55] D. Goulding, S. P. Hegarty, O. Rasskazov, S. Melnik, M. Hartnett, G. Greene, J. G. McInerney, D. Rachinskii, and G. Huyet, "Excitability in a quantum dot semiconductor laser with optical injection," *Phys. Rev. Lett.*, vol. 98, pp. 153903–, 2007.

[56] J. F. Heagy, N. Platt, and S. M. Hammel, "Characterization of on on–off intermittency," *Phys. Rev. E.*, vol. 49, no. 2, pp. 1140–1150, 1994.

[57] J. P. Nolan, *Stable Distributions - Models for Heavy Tailed Data*. Birkhauser, 2015.

[58] B. L. Lan, E. V. Yeoh, and J. A. Ng, "Distribution of detrended stock market data," *Fluct. Noise Lett.*, vol. 9, no. 3, pp. 245–, 2010.

[59] H. Wei, H. Xiao-Pu, Z. Tao, and W. Bing-Hong, "Heavy-tailed statistics in short-message communication," *Chin. Phys.*, vol. 26, no. 2, pp. 028902–, 2009.

[60] A. M. Segura, D. Calliari, H. Fort, and B. L. Lan, "Fat tails in marine microbial population fluctuations," *Oikos*, vol. 122, no. 12, pp. 1739–1745, 2013.

[61] J. P.Nolan, "Maximum likelihood estimation and diagnostics for stable distributions," in *Lévy Processes - Theory and Applications* (O. E. Barndorff-Nielsen, S. I. Resnick, and T. Mikosch, eds.), Birkhauser, 2001.

[62] J. P.Nolan, "Maximum likelihood estimation and diagnostics for stable distributions." http://academic2.american.edu/~jpnolan/stable/mle.pdf, 2001.

[63] J. P.Nolan, "Stable program." http://academic2.american.edu/~jpnolan/stable/stable.html, 2015.

[64] Y. Pomeau and P. Manneville, "Intermittency and the lorenz model," *Phys. Lett.*, vol. 75, no. 1, pp. 1–2, 1979.

[65] H. Fujisaka and T. Yamada, "A new intermittency in coupled dynamical systems," *Prog. Theor. Phys.*, vol. 74, no. 4, pp. 918–921, 1985.

[66] N. Platt, E. A. Spiegel, and C. Tresser, "On–off intermittency: a mechanism for bursting," *Phys. Rev. Lett.*, vol. 70, no. 3, pp. 279–282, 1993.

[67] N. Platt, S. M. Hammel, and J. F. Heagy, "Effects of additive noise on on–off intermittency," *Phys. Rev. Lett.*, vol. 72, no. 22, pp. 3498–3501, 1994.

[68] A. N. Pisarchik and V. J. Pinto-Robledo, "Experimental observation of two-state on–off intermittency," *Phys. Rev. E.*, vol. 66, pp. 027203–, 2002.

[69] R. Jaimes-Reategui and A. N. Pisarchik, "Control of on–off intermittency by slow parametric modulation," *Phys. Rev. E.*, vol. 69, pp. 067203–, 2004.

[70] P. W. Hammer, N. Platt, S. M. Hammel, J. F. Heagy, and B. D. Lee, "Experimental observation of on–off intermittency," *Phys. Rev. Lett.*, vol. 73, no. 8, pp. 1095–1098, 1994.

[71] Y. H. Yu, K. Kwak, and T. K. Lim, "On–off intermittency in an experimental synchronization process," *Phys. Lett. A*, vol. 198, no. 1, pp. 34–38, 1995.

[72] D. L. Feng, C. X. Yu, J. L. Xie, and W. X. Ding, "On–off intermittencies in gas discharge plasma," *Phys. Rev. E*, vol. 58, no. 3, pp. 3678–3685, 1998.

[73] T. John, U. Behn, and R. Stannarius, "Fundamental scaling laws of on–off intermittency in a stochastically driven dissipative pattern-forming system," *Phys. Rev. E*, vol. 65, pp. 046229–, 2002.

[74] A. Vella, A. Setaro, B. Piccirillo, and E. Santamato, "On–off intermittency in chaotic rotation induced in liquid crystals by competition between spin and orbital angular momentum of light," *Phys. Rev. E*, vol. 67, pp. 051704–, 2003.

[75] G. Verhille, N. Plihon, G. Fanjat, R. Volk, M. Bourgoin, and J. Pinton, "Large scale fluctuations and dynamics of the bullard - von kármán dynamo," *Geophys. Astrophys. Fluid. Dyn.*, vol. 104, pp. 189–205, 2010.

[76] J. L. Cabrera and J. G. Milton, "On–off intermittency in a human balancing task," *Phys. Rev. Lett.*, vol. 89, no. 15, pp. 158702–, 2002.

[77] T. Heil, I. Fischer, and W. Elsäßer, "Statistical properties of low-frequency fluctuations during single-mode operation in distributed-feedback lasers: experiments and modeling," *Opt. Lett.*, vol. 24, no. 18, pp. 1275–1277, 1999.

[78] A. N. Pisarchik and F. R. Ruiz-Oliveras, "Optical chaotic communication using generalized and complete synchronization," *IEEE J. Quantum. Electron.*, vol. 46, no. 3, pp. 279–284, 2010.

[79] S. H. Strogatz, "Death by delay," *Nature*, vol. 394, pp. 316–317, 1998.

[80] H. Haken, "Effect of delay on phase locking in a pulse coupled neural network," *Eur. Phys. J. B*, vol. 18, pp. 545–550, 2000.

[81] J. Weiner, R. Holz, F. W. Schneider, and K. Bar-Eli, "Mutually coupled oscillators with time delay," *J. Phys. Chem.*, vol. 96, no. 22, pp. 8915–8919, 1992.

[82] D. V. Ramana-Reddy, A. Sen, and G. L. Johnston, "Experimental evidence of time-delay- induced death in coupled limit-cycle oscillators," *Phys. Rev. Lett.*, vol. 85, pp. 3381–3384, 2000.

[83] T. Heil, I. Fischer, and W. Elsäßer, "Influence of amplitude-phase coupling on the dynamics of semiconductor lasers subject to optical feedback," *Phys. Rev. A*, vol. 60, no. 1, pp. 634–641, 1999.

[84] A. Hohl and A. Gavrielides, "Bifurcation cascade in a semiconductor laser subject to optical feedback," *Phys. Rev. Lett.*, vol. 82, no. 6, pp. 1148–1151, 1999.

[85] J. Zamora-Munt, C. Masoller, and J. García-Ojalvo, "Transient low-frequency fluctuations in semiconductor lasers with optical feedback," *Phys. Rev. A*, vol. 81, pp. 033820–, 2010.

[86] T. Heil, I. Fischer, and W. Elsäßer, "Chaos synchronization and spontaneous symmetry-breaking in symmetrically delay-coupled semiconductor lasers," *Phys. Rev. Lett.*, vol. 86, no. 5, pp. 795–798, 2001.

[87] E. A. Viktorov, A. M. Yacomotti, and P. Mandel, "Semiconductor lasers coupled face-to-face," *J. Opt. B: Quantum Semiclass. Opt.*, vol. 6, pp. L9–L12, 2004.

[88] G. Huerta-Cuellar, A. N. Pisarchik, A. V. Kir'yanov, Y. O. Barmenkov, and J. del Valle Hernández, "Prebifurcation noise amplification in a fiber laser," *Phys. Rev. E*, vol. 79, pp. 036204–, 2009.

[89] K. Pyragas, F. Lange, T. Letz, J. Parisi, and A. Kittel, "Stabilization of an unstable steady state in intracavity frequency-doubled lasers," *Phys. Rev. E*, vol. 61, no. 4, pp. 3721–, 2000.

[90] A. Pisarchik and B. Goswami, "Annihilation of one of the coexisting attractors in a bistable system," *Phys. Rev. Lett.*, vol. 84, no. 4, pp. 1423–, 2000.

[91] A. Pisarchik, "Controlling the multistability of nonlinear systems with coexisting attractors," *Phys. Rev. E*, vol. 64, pp. 046203–, 2001.

[92] A. Pisarchik and R. Jaimes-Reategui, "Intermittent lag synchronization in a nonautonomous system of coupled oscillators," *Phys. Lett. A*, vol. 338, no. 2, pp. 141–149, 2005.

[93] A. Pisarchik, R. Jaimes-Reategui, J. Villalobos-Salazar, J. H. García-López, and S. Boccaletti, "Synchronization of chaotic systems with coexisting attractors," *Phys. Rev. Lett.*, vol. 96, pp. 244102–, 2006.

[94] A. Pisarchik, R. Jaimes-Reategui, and J. Villalobos-Salazar, "Synchronization of multistable systems," *Int. J. Bif. Chaos*, vol. 18, no. 6, pp. 1801–, 2008.

[95] A. Pisarchik, ed., *Recent Achievements in Laser Dynamics: Control and Synchronization*. Research Singpost, 2008.

[96] F. Ruiz-Oliveras and A. Pisarchik, "Synchronization of semiconductor lasers with coexisting attractors," *Phys. Rev. E*, vol. 79, pp. 016202–, 2009.

[97] F. Ruiz-Oliveras, A. Pisarchik, C. Mirasso, and M. C. Soriano, "Phase-dependent synchronization of coupled semiconductor lasers," *Nonlinear Sci. Lett. B*, vol. 1, no. 2, pp. 69–76, 2011.

[98] L. Wu and S. Zhu, "Multi-channel communication using chaotic synchronization of multi-mode lasers," *Phys. Lett. A*, vol. 308, no. 2, pp. 157–161, 2003.

[99] K. Bar-Eli, "On the stability of coupled chemical oscillators," *Phys. D Nonlin. Phen.*, vol. 14, no. 2, pp. 242–252, 1985.

[100] D. Aronson, G. Ermentrout, and N. Kopell, "Amplitude response of coupled oscillators," *Phys. D Nonlin. Phen.*, vol. 41, no. 3, pp. 403–449, 1990.

[101] G. Ermentrout, "Oscillator death in populations of "all to all" coupled nonlinear oscillators," *Phys. D Nonlin. Phen.*, vol. 41, no. 2, pp. 219–231, 1990.

[102] P. Matthews and S. Strogatz, "Phase diagram for the collective behavior of limit-cycle oscillators," *Phys. Rev. Lett.*, vol. 65, no. 2, pp. 1701–, 1990.

[103] R. Mirollo and S. Strogatz, "Amplitude death in an array of limit-cycle oscillators," *J. Stat. Phys.*, vol. 60, no. 1, pp. 245–262, 1990.

[104] D. Ramana-Reddy, A. Sen, and G. Johnston, "Time delay induced death in coupled limit cycle oscillators," *Phys. Rev. Lett.*, vol. 80, no. 23, pp. 5109–5112, 1998.

[105] M. Yoshimoto, K. Yoshikawa, and Y. Mori, "Coupling among three chemical oscillators: Synchronization, phase death, and frustration," *Phys. Rev. E*, vol. 47, no. 2, pp. 864–, 1993.

[106] R. Herrero, M. Figueras, J. Rius, F. Pi, and G. Orriols, "Experimental observation of the amplitude death effect in two coupled nonlinear oscillators," *Phys. Rev. Lett.*, vol. 84, no. 23, pp. 5312–, 2000.

[107] D. Ramana-Reddy, A. Sen, and G. Johnston, "Experimental evidence of time-delay-induced death in coupled limit-cycle oscillators," *Phys. Rev. Lett.*, vol. 85, pp. 3381–3384, 2000.

[108] B. Kuntsevich and A. Pisarchik, "Synchronization effects in a dual-wavelength class-b laser with modulated losses," *Phys. Rev. E*, vol. 64, pp. 046221–, 2001.

[109] M. C. Soriano, F. Ruiz-Oliveras, P. Colet, and C. R. Mirasso, "Synchronization properties of coupled semiconductor lasers subject to filtered optical feedback," *Phys. Rev. E*, vol. 78, pp. 046218–, 2008.

[110] M. Crowley and I. Epstein, "Experimental and theoretical studies of a coupled chemical oscillator: phase death, multistability and in-phase and out-of-phase entrainment," *J. Phys. Chem.*, vol. 93, no. 6, pp. 2496–2502, 1989.